BBA - Molecular Basis of Disease 1869 (2023) 166711

Contents lists available at ScienceDirect

BBA - Molecular Basis of Disease

journal homepage: www.elsevier.com/locate/bbadis

# Stearoyl-CoA desaturase 1 deficiency exacerbates palmitate-induced lipotoxicity by the formation of small lipid droplets in pancreatic β-cells

Justyna Janikiewicz [a,*], Aneta M. Dobosz [a], Katarzyna Majzner [b], Tytus Bernas [c], Agnieszka Dobrzyn [a,*]

[a] Laboratory of Cell Signaling and Metabolic Disorders, Nencki Institute of Experimental Biology, Polish Academy of Sciences, Warsaw, Poland
[b] Faculty of Chemistry, Jagiellonian University, Jagiellonian Centre for Experimental Therapeutics (JCET), Cracow, Poland
[c] Department of Anatomy and Neurobiology, Virginia Commonwealth University School of Medicine, Richmond, USA

ARTICLE INFO

*Keywords:*
Type 2 diabetes
SCD1
Lipid droplets
β-Cells
Lipotoxicity
Pancreatic islets

ABSTRACT

The accelerating accumulation of surplus lipids in the pancreas triggers structural and functional changes in type 2 diabetes-affected islets. Pancreatic β-cells exhibit a restricted capacity to store fat reservoirs in lipid droplets (LDs), which act as transient buffers to prevent lipotoxic stress. With the increasing incidence of obesity, growing interest has been seen in the intracellular regulation of LD metabolism for β-cell function. Stearoyl-CoA desaturase 1 (SCD1) is critical for producing unsaturated fatty acyl moieties for fluent storage into and out of LDs, likely affecting the overall rate of β-cell survival. We explored LD-associated composition and remodeling in SCD1-deprived INS-1E cells and in pancreatic islets in wildtype and $SCD1^{-/-}$ mice in the lipotoxic milieu. Deficiency in the enzymatic activity of SCD1 led to decrease in the size and number of LDs and the lower accumulation of neutral lipids. This occurred in parallel with a higher compactness and lipid order inside LDs, followed by changes in the saturation status and composition of fatty acids within core lipids and the phospholipid coat. The lipidome of LDs was enriched in 18:2n−6 and 20:4n−6 in β-cells and pancreatic islets. These rearrangements markedly contributed to differences in protein association with the LD surface. Our findings highlight an unexpected molecular mechanism by which SCD1 activity affects the morphology, composition and metabolism of LDs. We demonstrate that SCD1-dependent disturbances in LD enrichment can impact pancreatic β-cells and islet susceptibility to palmitate, which may have considerable diagnostic and methodological value for the characterization of LDs in human β-cells in type 2 diabetes patients.

## 1. Introduction

Pancreatic β-cell failure is crucial for the development and progressive worsening of obesity-associated type 2 diabetes (T2D). It is notable, however, that pancreatic islets are exquisitely vulnerable to ensuing lipotoxicity and have a limited capacity to store surplus triglycerides (TGs) in lipid droplet (LD) depots [1]. Accumulating evidence shows that the ability of β-cells to alleviate lipotoxic stress is crucial for their functional recovery in T2D remission [2,3]. In particular, stearoyl-CoA desaturase 1 (SCD1) is the main metabolic control point that plays a pivotal role in the proper function and survival of β-cells under lipotoxic conditions [4]. Unsurprisingly, the undisturbed sequestration of excess fatty acids (FAs) by LDs is critical for cellular defense against lipid overload [5]. Notwithstanding the protective role of LD reservoirs for saturated fatty acids to mitigate their lipotoxic effect in pancreatic β-cells, this observation has become debatable [6,7].

*Abbreviations:* ABHD5, 1-acylglycerol-3-phosphate *O*-acyltransferase; ACAT1, acetyl-coenzyme A acetyltransferase 1; ACSL3, acyl-coenzyme A synthetase long chain family member 3; ATGL, adipose triglyceride lipase; CCTα, CTP:phosphocholine cytidylyltransferase α; CE, cholesteryl ester; CIDE-C, cell death inducing DFFA like effector C; CoA, coenzyme A; ELOVL6, elongation of long-chain fatty acids family member 6; FA, fatty acid; FFA, free fatty acid; GPAT4, glycerol-3-phosphate acyltransferase 4; HF, high fat; HSL, hormone-sensitive lipase; iPLA2, calcium-independent phospholipase A2; LD, lipid droplets; LPCAT1/2, lysophosphatidylcholine acyltransferase 1 or 2; MUFA, monounsaturated fatty acid; PA probe, push-pull pyrene probe; PC, phosphatidylcholine; PC-PLD2, phospholipase D2; PL, phospholipid; PLIN3, perilipin 3; PUFA, polyunsaturated fatty acid; SCD1, stearoyl-CoA desaturase-1; SFA, saturated fatty acid; T2D, type 2 diabetes; TG, triglyceride.

* Corresponding authors at: Laboratory of Cell Signaling and Metabolic Disorders, Nencki Institute of Experimental Biology, PAS, 3 Pasteur St, 02-093 Warsaw, Poland.

*E-mail addresses:* j.janikiewicz@nencki.edu.pl (J. Janikiewicz), a.dobrzyn@nencki.edu.pl (A. Dobrzyn).

https://doi.org/10.1016/j.bbadis.2023.166711
Received 13 December 2022; Received in revised form 28 March 2023; Accepted 30 March 2023
Available online 11 April 2023

Lipid droplets are dynamic organelles that integrate the collection, storage, trafficking, and signaling of neutral lipids in response to changes in energy demand [8]. A phospholipid (PL) monolayer surrounds a neutral core of TGs or cholesteryl esters (CEs) and is decorated with integral and peripheral proteins that are involved in lipid metabolism and regulate LD size, expansion, and degradation [9,10]. The impact of LDs on β-cell function is underappreciated, and studies of LD formation in primary pancreatic β-cells are extremely rare [2,11–13]. Effective LD buildup in β-cells was found in human islets from T2D donors or transplanted to immunodeficient NSG mice that were maintained on a high-fat (HF) diet, in functional islet β-like cells that were derived from human embryonic stem cells, and in dispersed rat islets that were subjected to lipotoxic insult [7,14,15]. High LD accumulation in β-cells was associated with insulin resistance, hyperglycemia, and a decrease in insulin secretion in T2D patients [16].

Enhanced palmitate incorporation into neutral lipid groups has been proposed as a mechanism of protection from lipotoxicity in cells with high SCD1 expression, including rodent and human pancreatic β-cells [5,17,18]. SCD1 catalyzes the introduction of the first double bond in the *cis*-Δ-9 position of palmitoyl-CoA (16:0) and stearoyl-CoA (18:0), thus generating palmitoleoyl-CoA (16:1n−7) and oleoyl-CoA (18:1n−9), respectively [19]. Ultimately, SCD1 activity remains indispensable for pancreatic β-cell survival through the control of insulin secretory capacity, DNA methylation patterns, cell identity status, and intracellular monounsaturated fatty acid/saturated fatty acid (MUFA/SFA) equilibrium [18,20,21]. Moreover, *SCD1* mRNA levels were upregulated in islets from prediabetic hyperinsulinemic ZDF rats, but they were downregulated in diabetic 12-week-old rodents that underwent islet failure [22] and in β-cell-enriched tissue from individuals with T2D [3]. In contrast, lower levels of SCD1 in insulin-secreting MIN6 and INS-1E cells increased endoplasmic reticulum stress and apoptosis in response to palmitic acid [22,23]. Additionally, the human EndoC-βH1 β-cell line was insensitive to the deleterious effect of stearate and palmitate unless SCD was silenced [18].

Interestingly, the importance of SCD1 in the remodeling of LDs was highlighted in various cell lines that were cultured from human hepatoma Huh7 cells [24,25], goat mammary epithelial cells [26,27], and mouse hepatocytes [28]. Hepatic seipin deficiency disrupted LD formation and homeostasis via SCD1 activity [28,29]. Moreover, SCD activity-deprived mutant nematodes exhibited difficulties in LD formation [30]. Considering that SCD1 is a pivotal metabolic checkpoint in handling β-cell lipid depots and functional failure, the unique strategy by which SCD1 governs the capacity to store and utilize LD remains incompletely understood. Our findings indicate that deficiencies in the enzymatic activity of SCD1 assist in the regulation of LD biogenesis, architecture, and metabolism. Biochemical, imaging, and functional studies revealed an unexplored phospholipid composition-dependent mechanism that regulates the size and lipid content of LDs during FA-induced dysfunction in pancreatic β-cells and murine islets. These changes accentuate the determination for a better understanding of the dynamics and metabolism of LD during lipotoxicity in pancreatic β-cells.

## 2. Materials and methods

### 2.1. Animals, dietary regimen, and isolation of pancreatic islets

Ten-week-old male C57BL/6J (WT) and SCD1-deficient ($SCD1^{-/-}$) age-matched mice on an identical C57BL/6J background ($n = 6$) were housed under pathogen-free conditions at 21 °C ± 1 °C under a 12 h/12 h light/dark cycle and fed ad libitum with standard laboratory chow (Ssniff, Germany, catalog no. V153x) or a high fat diet (60 % calories from fat; Ssniff, catalog no. E15742-34) for 6 weeks. The *Scd1* global knockout mice were generated as described previously [31].The animals were sacrificed by cervical dislocation. Pancreatic islets were isolated via intraductal infusion with ice-cold collagenase (Sigma, St. Louis, MO, USA) on a histopaque-1077 gradient (Sigma) as previously reported [21]. Isolated islets were snap frozen and stored at −80 °C until further use. All experimental procedures were approved by the First Local Ethical Committee for Animal Experiments in Warsaw (permit no. 37/2016, approved January 21, 2016).

### 2.2. Materials

The following antibodies: ATGL (catalog no. 2138), CCTα (catalog no. 6931), HSL (catalog no. 18381), and Rab11 (catalog no. 5589) were obtained from Cell Signaling Technology (Hertfordshire, UK). ABHD5 (catalog no. sc-376931), CIDE-C (catalog no. sc-517232), group VI $iPLA_2$ (catalog no. sc-376563), LPCAT2 (catalog no. sc-514354), PLIN3 (catalog no. sc-390968), and PC-PLD2 (catalog no. sc-515744) were purchased from Santa Cruz Biotechnology (Santa Cruz, CA, USA). PLIN2 (catalog no. GP40) and PLIN5 (catalog no. GP31) were obtained from PROGEN (Heidelberg, Germany). ACAT1 (catalog no. NBP1-89285) and ACSL3 (catalog no. NBP2-15252) were obtained from Novus Biologicals (Abingdon, UK). LPCAT1 (catalog no. 66044-1-Ig) was purchased from Proteintech (Manchester, UK). β-Actin (catalog no. 3854), β-tubulin (catalog no. T0198), and GPAT4 (catalog no. HPA016471) antibodies were obtained from Sigma (St. Louis, MO, USA). Peroxidase-conjugated goat anti-rabbit IgG (catalog no. 674371), goat anti-mouse IgG (catalog no. 115-035-146), and goat anti-guinea pig IgG (catalog no. A18769) secondary antibodies were purchased from MP Biomedicals (Irvine, CA, USA), Jackson ImmunoResearch Laboratories (West Grove, PA, USA), and ThermoFisher Scientific (Waltham, MA, USA), respectively. All other chemicals and reagents, unless otherwise specified, were obtained from Sigma.

### 2.3. Cell culture and chronic treatments

The rat insulinoma INS-1E β-cell line (a gift from Dr. Pierre Maechler, University of Geneva, Geneva, Switzerland) was cultured in complete RPMI 1640 medium that contained 5 % heat-inactivated fetal bovine serum, 1 mM sodium pyruvate, 50 μM 2-mercaptoethanol, 2 mM glutamine, 10 mM HEPES, 100 U/ml penicillin, and 100 μg/ml streptomycinin in a 5 % $CO_2$ atmosphere at 37 °C. To inhibit the enzymatic activity of SCD1, INS-1E cells were preincubated with 2 μM of the SCD1 inhibitor A939572 (Biofine International, Blain, WA, USA) for 4 h and then subjected to co-supplementation with 0.4 mM palmitic acid-BSA conjugate for the following 16 h. The incubation time with palmitate has been selected based on the CellTiter-Blue® Cell Viability assay. A 0.4 mM dose of palmitic acid was the maximal dose which did not significantly reduce cell numbers at 16 h after treatment.

Dimethylsulfoxide (DMSO) was applied as a vehicle control. For siRNA-mediated knockdown, the cells were reverse-transfected with 60 ng of siRNA against SCD1 (catalog no. 4390816, ID: s73339, Ambion, Houston, TX, USA) or Silencer Negative Control #1 siRNA (catalog no. AM4635, Ambion) for 72 h using Lipofectamine 2000 (0.5 μl/$cm^2$; Invitrogen). Palmitic acid was added for the last 16 h before sample collection. The desaturation index as an indicator of the enzymatic activity of SCD1 was determined after administration of the SCD1 inhibitor or siRNA as described previously [20,21]. Control cells for palmitate treatment were INS-1E cells that were incubated in medium that was supplemented with 7.5 % BSA.

### 2.4. Immunofluorescence

INS-1E cells that were grown on 0.001 % poly-L-ornithine-precoated coverslips were fixed with 3 % paraformaldehyde for 30 min at room temperature and then permeabilized with 0.3 % Triton X-100 for 10 min. Next, the cells were washed with phosphate-buffered saline (PBS) four times, and neutral lipids in LDs were stained with a 0.075 μg/ml solution of BODIPY 493/503 (Molecular Probes) in PBS for 50 min. Coverslips were washed three times, 5 min each, in PBS and then mounted on slides using ProLong Diamond Antifade Mountant with

DAPI (Life Technologies) before imaging using an Olympus BX41 confocal microscope. The diameters and numbers of LDs were measured with Olympus cellSens software. The LD diameters were divided into three size categories (≤1 μm, 1–3 μm and ≥3 μm) to evaluate their percentage fractions of total LDs. Furthermore, LD above 1 μm was split into three groups to quantify the percent range of LD diameters and an average diameter, respectively. A minimum of 60 cells were analyzed for each experimental condition from at least 30 individual snapshots.

### 2.5. Oil Red O staining

INS-1E cells were washed twice with PBS and then fixed in 4 % paraformaldehyde for 20 min. After two washes, the cells were air-dried and stained with freshly prepared Oil Red O solution (0.4 % Oil Red in isopropyl alcohol/water, 3:2) for 25 min at room temperature. Next, the stained INS-1E cells were washed five times with water and left in PBS, and images were acquired with an Olympus CKX41 bright-field microscope (Olympus). To quantify the intracellular enrichment of TGs, Oil Red O was extracted from the cells with 100 % isopropanol and assayed by measuring absorbance at 500 nm with a microplate reader (Infinite M200, Tecan, Männedorf, Switzerland). Next, the relative values of intracellular neutral lipid content were obtained after subtraction the background staining and normalization to the corresponding vehicle control or negative control siRNA, respectively. In the case of tissues, pancreatic cryostat sections (10 μm) were fixed for 20 min in 10 % buffered formalin, extensively rinsed with tap water, and stained with freshly prepared Oil Red O solution as above at room temperature for 4 h. The Oil Red O reaction was followed by hematoxylin staining, and sections were mounted in Dako Faramount Aqueous Mounting Medium (Dako).

### 2.6. Isolation of LDs

INS-1E cells were cultured in three-layer 525 $cm^2$ flasks (BD Falcon) and treated as described above. Lipid droplets were isolated by density gradient centrifugation as previously described [32]. Briefly, INS-1E cells were washed twice with PBS and resuspended in 1 ml of ice-cold hypotonic lysis medium (HLM; 20 mM Tris-HCl [pH 7.4], 1 mM ethylenediaminetetraacetic acid [EDTA], and 10 mM sodium fluoride), supplemented with 10 μg/μl leupeptin, 5 μg/μl pepstatin A, 2 μg/μl aprotinine, 1 mM sodium orthovanadate, and 1 mM phenylmethylsulfonyl fluoride (PMSF). Next, the cells were homogenized in a Potter-Elvehjem tissue homogenizer with gentle strokes on ice. The homogenate was then centrifuged at 1000 ×*g* for 10 min at 4 °C, and the supernatant was adjusted to 20 % sucrose with ice-cold HLM medium that contained 60 % sucrose. The mixture was first overlaid with 5 ml of ice-cold HLM that contained 5 % sucrose, followed by 5 ml of ice-cold HLM. Tubes were centrifuged at 28,000 ×*g* for 45 min at 4 °C in a SW41Ti rotor (Beckman). The white top layer of the gradient that corresponded to the LD fraction was harvested and stored at −80 °C before further analysis.

### 2.7. Protein samples and immunoblotting analysis

To fully recover proteins from frozen LD fractions, they were delipidated with ice-cold acetone overnight at −20 °C, followed by sequential washes in acetone/ether (1:1, v/v) and ether, resuspended in 2× Laemmli sample buffer, and sonicated at 60 °C for 4 h. In the case of INS-1E cells after treatment and isolated pancreatic islets, the collected samples were lysed for 30 min in ice-cold buffer (50 mM Tris-HCl, 5 mM EDTA, 1 % Triton X-100, and 150 mM NaCl) that was co-supplemented with protease (10 μg/μl leupeptin, 5 μg/μl pepstatin A, 2 μg/μl aprotinine, and 1 mM PMSF) and phosphatase (1 mM sodium orthovanadate and 10 mM sodium fluoride) inhibitors. Next, the lysates were centrifuged at 10,000 × *g* at 4 °C for 25 min, and total protein content in the supernatants (whole-cell lysates) was determined using the Bio-Rad protein assay (Bio-Rad, Hercules, CA, USA) with BSA as the reference. All types of protein lysates were mixed with 4× Laemmli sample buffer, separated on 10 % SDS-PAGE gels, and transferred to polyvinylidene difluoride membranes (Millipore, Billerica, MA, USA). After blocking with 5 % nonfat milk or 5 % BSA, membranes were probed with appropriate primary and horseradish peroxidase-conjugated secondary antibodies, respectively. The bands were visualized using SuperSignal West Pico PLUS Chemiluminescent Substrate (ThermoFisher Scientific). Protein levels were quantified by densitometry and expressed relative to the abundance of β-actin in the case of the extracts from INS-1E cells or β-tubulin when immunoblotting was performed on lysates from the murine pancreatic islets.

### 2.8. Propargylcholine incorporation assay

The de novo synthesis of PC (phosphatidylcholine) was quantified using a click-chemistry reaction. Briefly, after treating INS-1E cells as described above, propargylcholine (Jena Bioscience, Jena, Germany, 10 μM) was added simultaneously with palmitate for 16 h. The cells were then fixed with 4 % paraformaldehyde for 20 min and permeabilized in 1 % FA-free BSA with 0.1 % saponin for 10 min, and the click-chemistry reaction was immediately conducted with Alexa Fluor 488 Azide (Jena Bioscience) using the Click-iT Cell Reaction Buffer Kit (Invitrogen) according to the manufacturer's guidelines. Fluorescence was quantified with a Tecan Infinite M200 microplate reader.

### 2.9. Push-pull pyrene dye visualization

INS-1E cells were cultured on 35 mm glass-bottom dishes with 20 mm bottom wells (Cellvis, Sunnyvale, CA, USA) that were precoated with 0.001 % poly-L-ornithine. A freshly prepared solution of the PA probe (push-pull pyrene probe) in RPMI was added to the cells (50 nM) and incubated for 3 min in the dark at room temperature as previously described [33]. The obtained samples were immediately imaged in serum-free RPMI medium. Images of cell midsections were recorded using a Leica SP8 confocal microscope with a 63× oil immersion Plan Apo objective lens (NA = 1.4). The microscope system was equipped with an acousto-optical beam splitter (AOBS) and two hybrid detectors (HyD), working in the integration mode. The fluorescence of PA was excited with a 405 nm light (5 mW diode laser) and detected simultaneously in two bands: 450–550 nm (ordered lipid phase) and 575–675 nm (disordered phase). The emission of PA was recorded using a rotating polarizer in two directions: parallel ($\parallel$) and perpendicular ($\perp$) to the main polarization axis of the excitation beam. The pixel size was 90 nm in the x-y plane, corresponding to a 25 × 25 μm field of view. The pixel dwell time was 1.12 μs, and the confocal pinhole was set to 1 Airy unit (at 530 nm). A series of three image sets (four fluorescence and one transmitted light) was collected from every view and averaged. Each experimental group comprised 75–100 cells. The PA fluorescence images were processed with a median filter (3 × 3 size). The background was estimated as a minimum of the average intensity in a 25 × 25 region and subtracted from each fluorescence channel. Images of the ordered/unordered lipid phase concentration ratio were estimated with GP using the following formula [34]:

$$GP = \frac{I_{500} - I_{625}}{I_{500} + I_{625}} \quad (1)$$

where $I_{500}$ and $I_{625}$ are pixel sums ($\parallel$ and $\perp$ polarizations) of the short (ordered phase) and long (unordered phase) emission wavelengths. The fluidity of these two membrane phases was estimated with respective images of steady-state anisotropy using the following formula:

$$R = \frac{I_{\parallel} - G^{*}I_{\perp}}{I_{\parallel} + 2^{*}G^{*}I_{\perp}} \quad (2)$$

where G is the detection sensitivity factor, $I_{\parallel}$ is fluorescence measured in

the direction parallel to excitation, and I⊥ is the perpendicular counterpart of the short and long wavelength emission bands. The G factor (0.98) was calculated using a 1 mM solution of fluorescein in PBS (pH 7.4, 37 °C), imaged under the same conditions as PA. Regions that corresponded to the cells were isolated from images with a static threshold (5 intensity units), followed by morphological closing (three iterations). Histograms of total fluorescence intensities (four channels combined) of pixels that belonged to the masks were divided into five equal quantiles. The distributions of GP and anisotropy were constructed using pixels that corresponded to the 5th intensity quantile.

### 2.10. Raman measurements

For Raman analysis, cells were directly grown on 0.001 % poly-L-ornithine-coated calcium fluoride discs (25 × 2 mm, Crystran LTD, Poole, UK) that were placed in a six-well plate until they reached 70 % confluence. After the aforementioned treatments, the cells were fixed for 20 min with 4 % paraformaldehyde, rinsed, and stored at 4 °C in PBS until data acquisition from at least 20 cells per experimental group as previously described [35]. Briefly, Raman spectroscopic mapping was performed using the Confocal Raman Imaging system (WITec alpha 300), which was supplied with air-cooled solid-state lasers that operated at 532 nm. Imaging was performed with a 63× water immersion objective (Zeiss Fluor, NA = 1.0). The scattered light was directed to the spectrometer using a 50 μm core diameter multimode fiber, which also acted as the pinhole for confocal detection. The spectrometer (WITec UHTS300) was equipped with a black-illuminated CCD camera (Andor, DU401A-BV-352) and 600 grooves/mm grating (BLZ = 500 nm). Spectral measurements of INS-1E cells were performed with an integration time of 0.5 s per spectrum, sampling density of 0.5 μm, and laser excitation wavelength of 532 nm (laser power of ca. 15–20 mW at the sample position). All spectra were acquired in the 100–3600 $cm^{-1}$ spectral range with 3 $cm^{-1}$ spectral resolution. Data acquisition was controlled by the WITec Suite Five software package. Preprocessing included cosmic spike removal and background subtraction (polynomial, order 3) and was performed using WITec Suite Five software. Chemical images were generated by the integration of selected marker bands using a sum filter. For data exploration, a k-means cluster analysis (KMCA) was conducted. The aim of KMCA was to group the analyzed objects (spectra) into clusters; hence, similar spectra were gathered within the same group. This approach enables the extraction of averaged spectra from cell organelles that vary in biochemical composition, a reduction of the tremendous number of single spectra, and the visualization of cell classes. For the KMCA analysis of Raman spectra of single cells, the object–centroid distance was calculated according to the Manhattan (city block) method.

### 2.11. Lipid isolation and analysis

Lipids were extracted from isolated LDs or pancreatic islets using the method of Bligh and Dyer [36] and separated on silica gel 60 thin-layer chromatography plates (Merck, Darmstadt, Germany) with n-heptane/isopropyl ether/glacial acetic acid (60/40/3, v/v/v) for neutral lipids or chloroform/methanol/acetic acid/water (50/37.5/3.5/2, v/v/v/v) for PLs. To visualize lipid bands, the silica plate was soaked in a mixture of 10 % cupric sulfate and 8 % phosphoric acid in water, followed by incubating at 140 °C for 20 min. The relative lipids were then measured by densitometry using ImageJ software. For the FA content analysis, bands that corresponded to the TG, CE, and PC standards were visualized with 0.2 % 2,3-dichlorofluorescein, scraped off the plate, and transmethylated in the presence of 14 % boron trifluoride in methanol. The resulting FA methyl esters were extracted with hexane and subjected to GC–MS (Agilent 7890A-5975C equipped with an Agilent 19091N-205 capillary column, Agilent Technologies, Santa Clara, CA, USA). Peak alignment, purity, and quality analyses were performed using Agilent MSD Productivity ChemStation software. Methyl nonadecanoate was used as an internal standard for further compound quantification by selected ion monitoring.

### 2.12. RNA extraction and qRT-PCR

Total cellular RNA from pancreatic islets was extracted with QIAshredder homogenizers and the RNeasy Micro Kit (Qiagen, Hilden, Germany) according to the manufacturer's recommendations. DNase-treated RNA (1 μg) was reverse-transcribed into cDNA using the High Capacity cDNA Reverse Transcription Kit with RNase inhibitor and random primers (Applied Biosystems, Thermo Fisher Scientific, Pittsburgh, PA, USA). The quantitative real-time PCR (qRT-PCR) was performed with SsoAdvanced Universal SYBR SMX (Bio-Rad, Hercules, CA, USA) on a CFX Connect Real-Time PCR Detection System (Bio-Rad, Hercules, CA, USA). Relative mRNA levels were determined by the ΔΔCt method and normalized to the internal reference of murine *Rps17*. The sequences of primers are listed in Supplementary Table 1.

### 2.13. Statistical analysis

The statistical analysis was performed using GraphPad Prism 8.3.0 software. Data throughout the study are presented as means ± SD and the experiments were performed in triplicate unless stated otherwise. Statistical significance was assessed using one-way analysis of variance followed by Dunnett's or Tukey's post hoc test. Values of $p < 0.05$ were considered statistically significant.

## 3. Results

### 3.1. Inhibition of SCD1 activity affects neutral lipid storage in INS-1E cells

Considering that the desaturation activity of SCD1 remains the main brake on free fatty acid (FFA) toxicity in human and rodent β-cells, it ameliorates the deleterious effect of palmitic acid, which is the most prevalent SFA in the human body [18,37,38]. The mechanism by which SCD1 prevents lipotoxicity involves an undisturbed capacity of TG storage, which is believed to be protective for β-cells [5,18]. To test whether desaturase activity is necessary for the accumulation of neutral lipids, we performed the Oil Red O staining of INS-1E cells that were subjected to either treatment with the selective pharmacological SCD1 inhibitor A939572 or the genetic ablation of SCD1 using siRNA as described previously [20,21]. The partitioning of Oil Red O into neutral lipids was then also examined after 16 h of palmitate (16:0) co-supplementation (Fig. 1A and B). Compared with controls, the quantification of Oil Red O staining demonstrated the extensive accumulation of intracellular TGs after palmitate treatment. Interestingly, Oil Red O intensity significantly decreased by over 13 % in the chemically or genetically deprived SCD1 groups compared with the supplementation of INS-1E cells with 16:0 alone (Fig. 1C and D). Ultimately, the decrease in Oil Red O enrichment in samples with the downregulation of SCD1 activity reflects aberrant cellular lipid storage capacity and is consistent with lower desaturation in these cells [20,21].

### 3.2. Decrease in SCD1 activity alters lipid droplet morphology and size

To further test whether diminished SCD1 activity/expression correlates with LD abundance, we visualized LDs by staining INS-E cells with BODIPY 493/503 and then monitored the number and size of LDs. INS-1E cells that were exposed to 16:0 treatment were characterized by a substantial increase in the abundance of LDs per cell. In the simultaneous presence of a SCD1 inhibitor or after silencing the expression of *SCD1*, the number of BODIPY 493/503-stained LDs decreased by over 30 % and 10 %, respectively (Fig. 2A and E). Phenotypically, the deficiency of SCD1 activity was accompanied by the appearance of numerous round but smaller LDs through a substantial shift in LD

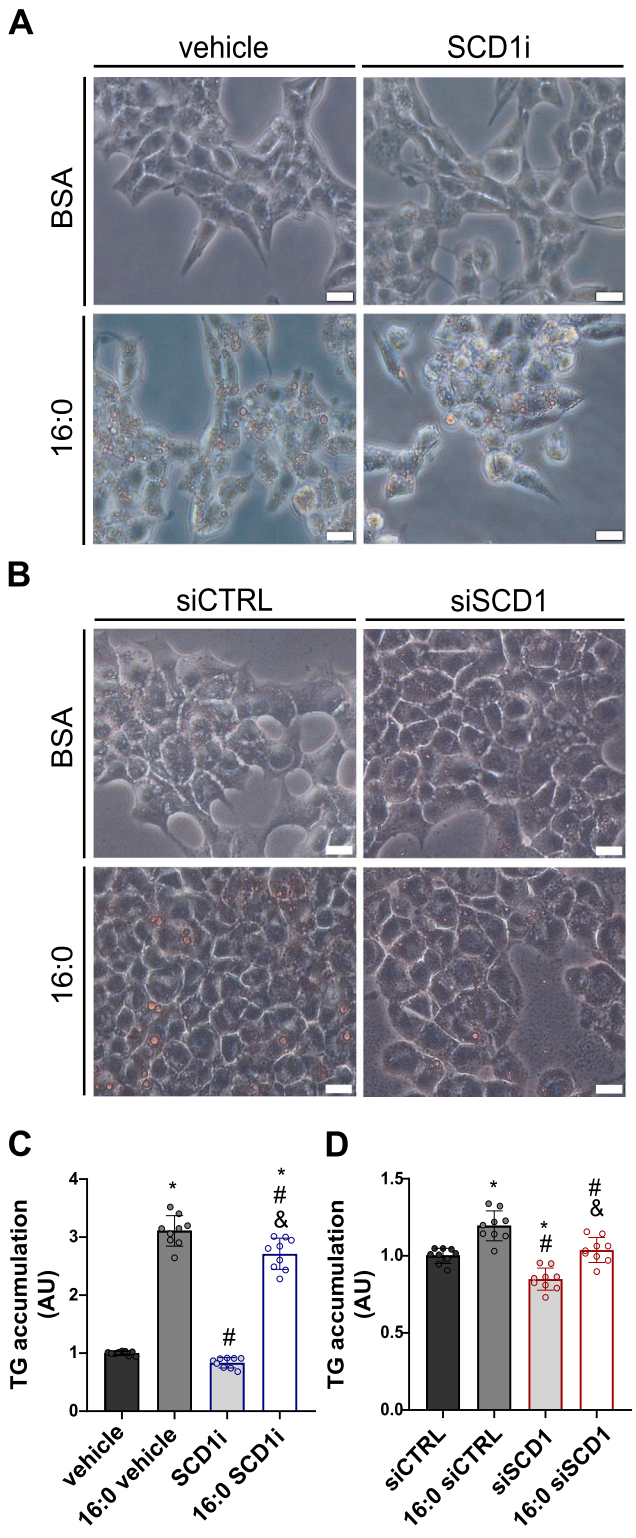


**Fig. 1.** Downregulation of SCD1 enzymatic activity lowers intracellular lipid stores in Oil Red O-stained INS-1E cells. INS-1E cells were subjected to SCD1 inhibition with A939572 (SCD1i) (A) or transiently silenced with siRNA against SCD1 (siSCD1) (B) and palmitate treatment (16:0). Lipid droplets were extracted using isopropanol. (C, D) The quantitative data from Oil Red O intensity are expressed as the mean ± SD of three independent experiments done in triplicates ($n = 9$). Intracellular lipid stores were normalized in relation to either vehicle or siCTRL negative controls, respectively. Scale bar = 500 μm. $^{*}p < 0.05$, vs. vehicle/siCTRL; $^{\#}p < 0.05$, vs. 16:0 vehicle/16:0 siCTRL; $^{\&}p < 0.05$, vs. SCD1i/siSCD1.

diameter from a large size (≥3 μm) and medium size (1–3 μm) toward very small droplets (≤1 μm; Fig. 2B and F). Furthermore, when we split LD diameters > 1 μm into three categories, the prevalence of very large LDs was 27 % for palmitic acid treatment and nearly 15 % for palmitate and SCD1 inhibitor co-supplementation (Fig. 2C). Ultimately, LD diameters were considerably smaller, with an average size of 2.30 and 2.14 μm, respectively (Fig. 2D). The pattern and frequency of diameter distribution among the three categories was similar in the presence of 16:0 treatment vs. the simultaneous supplementation of palmitate and silencing of SCD1 (Fig. 2G). Additionally, the average LD diameter of bodies that were >1 μm was 2.03 and 1.83 μm, respectively (Fig. 2H). Collectively, these results indicate that the deficiency of SCD1 activity affects the amount and size of LD but does not compromise the ability of INS-1E cells to generate LD in the lipotoxic milieu.

### 3.3. SCD1 affects the fluidity and compactness of lipid droplets

Because of their substantial TG and CE content, LDs are highly hydrophobic and the most apolar intracellular lipid structures [33,38]. Given the significant changes in LD abundance, we next investigated the biophysical status and compactness of LDs using a membrane probe for lipid domains. The push-pull pyrene (PA) probe shifts its emission in response to changes in membrane hydration and solvent relaxation, which are lipid order-linked indicators [33,34]. The fluorescence of PA was detected simultaneously in two bands of ordered/disordered lipid phases, demonstrating that various lipid-containing cellular structures were labeled by the dye in palmitate-treated INS-1E cells. Lipid droplets appeared as the brightest signal in the cytoplasm (Supplementary Fig. 1A). Based on the ratio of PA emission intensities, generalized polarization (GP) values enabled the assessment of membrane fluidity within lipid domains (Fig. 3A). The treatment of INS-1E cells with palmitate for 16 h made the plasma membranes less fluid (GP = 0.466); hence, the inside of LDs was very compact and close to the liquid ordered phase (Fig. 3C). Interestingly, LDs in cells with low SCD1 activity and co-supplemented with 16:0 were more ordered and stiff (GP = 0.334). Moreover, anisotropy values in the hydrophobic surrounding (Fig. 3B) showed significantly lower mobility of the PA probe in these LDs (R = 0.188) compared with the LDs of palmitate-treated INS-1E cells (R = 0.164; Fig. 3D).

Next, to further investigate the impact of SCD1 inhibition on LD remodeling in the β-cell lipidome under palmitate overload conditions, we used linear RAMAN imaging spectroscopy, which allows a focus on the complexity, biochemical composition, and alterations of LD [40]. Confocal measurements confirmed that LDs of INS-1E cells that were incubated with 0.4 mM palmitic acid handled the high influx of 16:0 by incorporating it into various lipid functional classes that co-exist inside lipid bodies (Supplementary Fig. 1B and C). The average RAMAN spectra from the LD groups correlated well with the spectra of analytical standards of selected saturated and unsaturated FAs or selected lipid species (Fig. 3E and F). The mean spectral profile of the LD class from palmitate-exposed INS-1E cells was dominated by marker bands of SFA (1003, 1060, 1128, and 1295 $cm^{-1}$), suggesting the enrichment of these LDs in stearate and palmitate moieties (Fig. 3G and H). Furthermore, fingerprints of phospholipids and cholesteryl esters occurred as marker bands at 716 $cm^{-1}$ (C—N symmetric stretching of the choline group) and 1740 $cm^{-1}$ (C═O vibration), respectively. Additionally, LDs in both groups contained protein components because of the presence of a band at 1660 $cm^{-1}$ (amide I) and bands in the spectral range of 1200–1400 $cm^{-1}$ (amide III) (Fig. 3G and H). Unsaturated FAs were identified in RAMAN spectra bands at 1656, 2847, and 3009 $cm^{-1}$ because of the stretching mode of =C−H that was associated with C═C double bonds, whereas bands at 1444 $cm^{-1}$ corresponded to the $CH_2$ bending vibration of saturated lipids. For average spectra of LDs from cells that were exposed to simultaneous treatment with palmitate and pharmacological or genetic SCD1 deprivation, the unsaturation ratio (1660/1444 $cm^{-1}$) equaled 0.459 and 0.667, respectively (Fig. 3I and J)

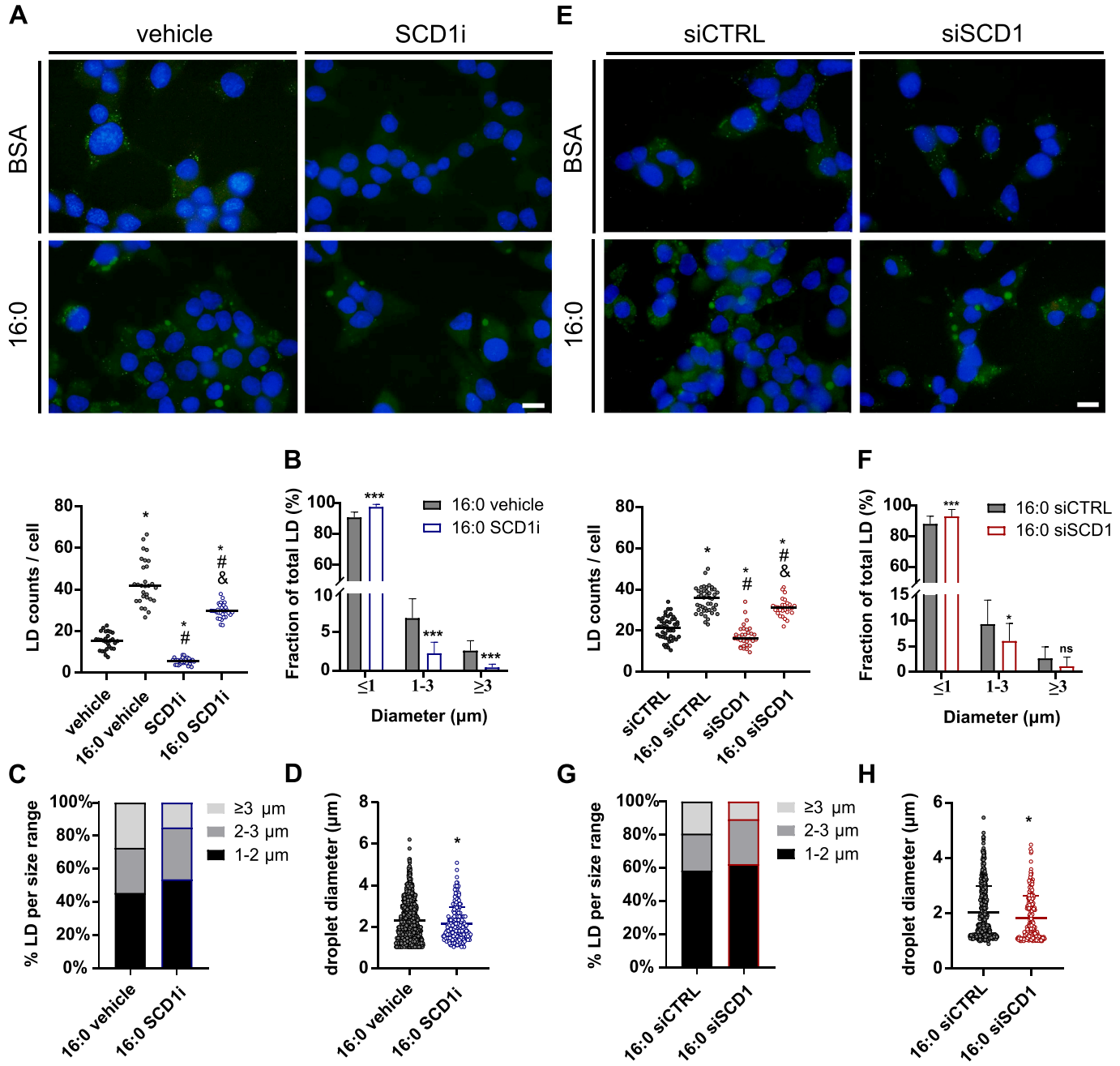


**Fig. 2.** Intracellular lipid droplet number and size are altered upon the deficiency of SCD1 activity. Representative images of the cellular phenotype of INS-1E cells that were incubated with the SCD1 inhibitor A939572 (A) or transfected with *SCD1*-targeting siRNA (E) and treated (or not) with 0.4 mM palmitate. Lipid droplets and nuclei were visualized with BODIPY 493/503 (green) and 4,6-diamidino-2-phenylindole (DAPI; blue), respectively. Scale bars = 10 μm. The data are expressed as the mean number of LDs/cell ± SD of three independent experiments, calculated from at least 60 cells in each experimental group. The measurements were taken from a minimum of 30 individual snapshots per experimental condition. $^{*}p < 0.05$, vs. vehicle/siCTRL; $^{\#}p < 0.05$, vs. 16:0 vehicle/16:0 siCTRL; $^{\&}p < 0.05$, vs. SCD1i/siSCD1. Lipid droplet morphology was quantified as the percentage (B, F) of small size (≤1 μm), medium size (1–3 μm), and supersized droplets (≥ 3 μm) from the total number of LDs ($^{*}p < 0.05$, $^{***}p < 0.001$, ns = not significant, compared with matched controls). The percent range of LD diameters was categorized into three groups from LDs whose diameter was larger than 1 μm (C, G). An average diameter of a LD above 1 μm was also quantified within the experimental groups (D, H). $^{*}p < 0.05$, vs. 16:0 vehicle/16:0 siCTRL.

Thus, LDs that were isolated from INS-1E cells that were subjected to palmitate treatment and SCD1 deprivation exhibited a slightly higher degree of unsaturation than LDs from cells that were incubated with palmitic acid alone (ratio = 0.381 and ratio = 0.627). Additionally, low-intensity marker bands at 1067, 1095, and 1132 $cm^{-1}$ (*trans*, *gauche*, *trans* stretching vibration C—C) were shifted to the lower wave numbers, indicating a more complex LD structure and the presence of phospholipids, possibly phosphatidylcholine with an incorporated 16:0 moiety (Fig. 3G and H). These results correspond to enrichment of the LD mantle in phosphatidylcholine (PC), which consists of unsaturated moieties [41]. Altogether, the combined PA fluorescence and RAMAN analyses demonstrated an increase in biochemical LD remodeling in palmitate-treated INS-1E cells with diminished SCD1 activity compared with challenging cells with palmitic acid alone.

### 3.4. Deficiency in SCD1 changes metabolic profile of LD in β-cells

To verify whether apart from morphology, the enzymatic deficiency of SCD1 affects the lipid profile of LDs, we isolated LDs by centrifugation on a sucrose gradient, and lipid classes were separated by thin-layer chromatography (TLC). In mammalian cells, the primary neutral lipids of the LD core are stored at various ratios, whereas PC is the most prominent phospholipid in the LD membrane, ranging up to 60 % of the total phospholipid mantle [8,42]. Indeed, we found that LD fractions from INS-1E cells were enriched in CE, TG, and PC (Fig. 4A and B). The TLC data corroborated the imaging results. CE levels in LDs from INS-1E cells that were subjected to SCD1 inhibition or transiently silenced with siRNA against SCD1 (siSCD1) and palmitate treatment (16:0) were >30 % and 40 % lower compared with control cells (Fig. 4C). Accordingly, lipid droplet phenotypes of cells that were pharmacologically or genetically deprived of SCD1 activity exhibited more than a 33 % and 47 % drop in relative TG levels, whereas TG content in LDs after palmitic acid treatment was >36 % and 88 % higher than in control cells, respectively (Fig. 4D). Palmitate treatment significantly increased PC content in INS-1E cells, whereas co-supplementation with the SCD1 inhibitor or transfection with a siRNA against SCD1 resulted in the further accumulation of PC by 49 % and 21 %, respectively (Fig. 4E). This observation was complementary to the overall upregulation of PC synthesis, reflected by the significant increase in propargylcholine incorporation by the click-chemistry reaction in INS-1E cells (Supplementary Fig. 2A). In fact, the effect of enzymatic SCD1 depletion on LD size was attributable to the decrease in the overall TG and CE fraction. Notably, these cells had more LD-associated PC compared with LDs from corresponding controls, indicating a key role for SCD1 in LD expansion and stability.

### 3.5. Lipid droplet size is associated with TG saturation status and PC composition

Differences in LD formation and size correlate with alterations in TG storage and changes in composition and stability of the phospholipid envelope [43,44]. To further determine whether SCD1 regulates LD size through adjustments in saturation and FA content, we assessed the FA composition of TG, CE, and PC in freshly isolated LDs by gas chromatography–mass spectrometry (GC–MS). The lipidomic analysis of most abundant fatty acids in TGs revealed higher levels of 16:0, 16:1, 18:0, 18:1, 20:4n−6, 20:5n−3, and 20:3n−6 species in palmitate-supplemented cells alone or in combination with the enzymatic and genetic inhibition of SCD1 compared with control LDs (Fig. 5A). Accordingly, we detected reductions of the desaturation index—with a higher preference for 16:0 substrate—by >33 % and 23 % in cells after the combination of palmitate treatment and SCD1 inhibition or transient silencing with siSCD1, in contrast to incubation with palmitic acid alone (Fig. 5D). Furthermore, we observed that lipid CE components remained mostly unaffected between solely palmitate-incubated cells and treated in tandem with the enzymatic or genetic inhibition of SCD1 (Fig. 5B). This effect was followed by a decrease in SCD1 enzymatic activity with palmitic acid treatment or after co-exposing INS-1E cells to the SCD1 inhibitor/siRNA (Fig. 5E). In contrast, the lipidomic analyses of the PC fraction showed that cells subjected to SCD1 inhibition/transiently silenced with siRNA against SCD1 or co-supplemented with palmitate contained higher amounts of 16:1, 18:1, and 18:2n−6 FAs compared with the respective BSA control (Fig. 5C). The aforementioned FAs are mainly esterified at the *sn−2* position in PC [45]. This effect was followed by higher levels of ELOVL6 activity (elongation of long-chain fatty acids family member 6) and a decrease in the Δ5/6 desaturase index in cells that were treated in parallel with the SCD1 inhibitor or siRNA against SCD1 and palmitate (Supplementary Fig. 2B and C). Both ELOVL6 and Δ5/6 are crucial enzymes in polyunsaturated fatty acid (PUFA) conversion and the main determinants of cellular PUFA levels [46]. Collectively, these results suggest that saturation of the LD core depends on the enzymatic activity of SCD1, whereas the phospholipid mantle is instead determined by changes in FA composition than saturation status (Fig. 5F).

### 3.6. Manipulation of LD PC levels and composition alters protein repertoire at the LD surface

Lipid droplets are metabolically active hotspots for local lipid biosynthesis. Many enzymes need to translocate between the cytosol and LD surface to catalyze this complex activity [47]. We next investigated the abundance of well-established LD-associated proteins [48] that are involved in TG synthesis/nucleation (acetyl-CoA acetyltransferase 1 [ACAT1], glycerol-3-phosphate acyltransferase 4 [GPAT4]), the delivery of active fatty acyl-coenzyme A (CoA; ACSL3), and the control of LD size or structure (cell death inducing DFFA like effector C [CIDE-C], perilipin 2 [PLIN2], perilipin 3 [PLIN3]) in total lysates. In groups of INS-1E cells that were treated in parallel with the SCD1 inhibitor or siRNA against SCD1 and palmitic acid, the protein content of ACAT1 and GPAT4 compared with control cells decreased by 55 % and 70 % and by 56 % and 80 %, respectively (Fig. 6A and B). An average 52 % increase in the abundance of ACSL3 was confirmed in palmitate-incubated INS-1E cells, whereas simultaneous SCD1 deficiency led to a modest 16 % or 9 % increase in ACSL3 protein content, respectively (Fig. 6A and B). The levels of CIDE-C protein in samples that were exclusively treated with palmitate were greater than in untreated cells. This effect was further elevated as the protein content of CIDE-C, compared with control cells, increased nearly 16-fold and two-fold upon simultaneous treatment of INS-1E cells with palmitic acid and downregulation of SCD1 inhibition or SCD1 expression, respectively.

Moreover, PLIN2 protein levels closely correlate with LDs pool size and cellular TG contents, especially when β-cells or mouse and human islets were subjected to fatty acid loading in vitro [49,52]. An average two-fold increase in the abundance of PLIN2 was confirmed in palmitate-incubated INS-1E cells, whereas simultaneous SCD1 deficiency led to 56 % or 43 % decrease in PLIN2 protein content, respectively (Fig. 6A and B). Furthermore, the inhibition of SCD1 activity and downregulation of SCD1 gene expression in INS-1E cells increased PLIN3 protein levels nearly two- and four-fold compared with control cells. Incubation with palmitate alone increased the abundance of PLIN3 by approximately 50 %. However, no significant difference in PLIN3 protein content was observed between SCD1-deficient INS-1E cells and SCD1-deficient INS-1E cells that were treated with palmitate (Fig. 6A and B). PLIN3 is attached preferentially to the surface of small LDs enriched in unsaturated FA moieties [51]. These findings were consistent with the decreases in the size and number of LDs, supporting the metabolic inability to form large LDs in SCD1-activity/expression-deprived cells.

To investigate whether the observed rearrangements in PC FA composition determine the abundance of proteins that are involved in LD biogenesis and structure, we monitored levels of several proteins that are involved in PC synthesis and remodeling, including calcium-independent phospholipase A2 ($iPLA_2$), phospholipase D2 (PC-PLD2), CTP:phosphocholine cytidylyltransferase α (CCTα), lysophosphatidylcholine acyltransferase 1 (LPCAT1), and lysophosphatidylcholine acyltransferase 2 (LPCAT2) [41,47]. Both impairments in SCD1 activity and the downregulation of SCD1 gene expression increased $iPLA_2$ protein content nearly two-fold compared with control INS-1E cells, but parallel stimulation with palmitate increased $iPLA_2$ levels by approximately 56 % and 14 %, respectively (Fig. 6A and B). The abundance of PC-PLD2, which is responsible for PC degradation, decreased nearly 50 % in SCD1-deprived INS-1E cells. Nearly two-fold and barely one-fold decreases in PC-PLD2 content were observed in INS-1E cells that were simultaneously subjected to SCD1 deficiency and treated with palmitic acid compared with INS-1E cells that were treated palmitate alone (Fig. 6A and B). These data corroborated the higher abundance of LD-associated PC in the TLC analysis (Fig. 2). Interestingly, deficiencies of

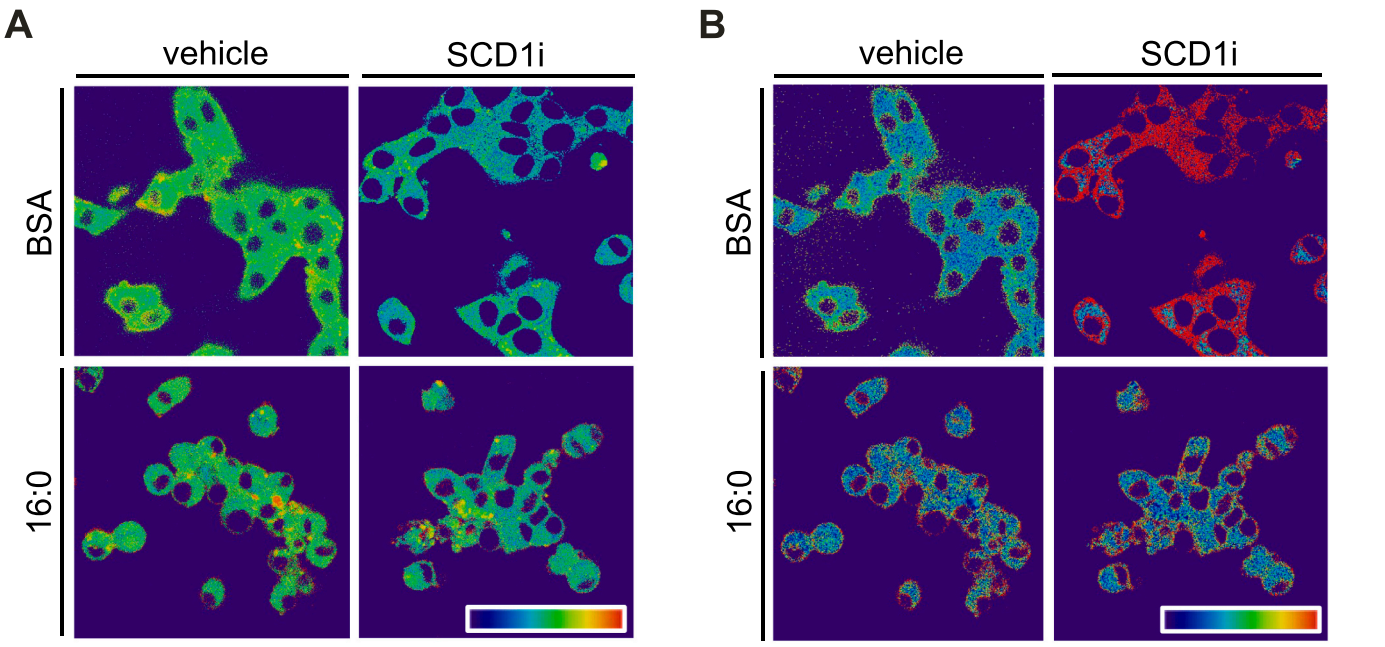


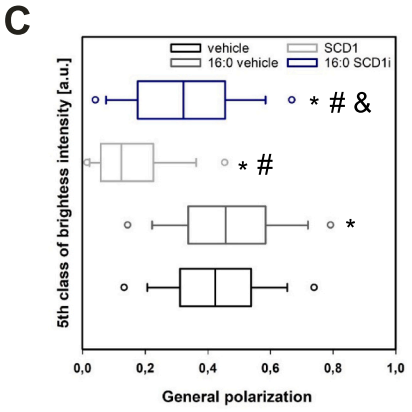


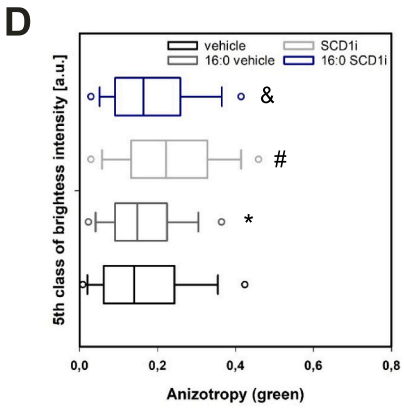


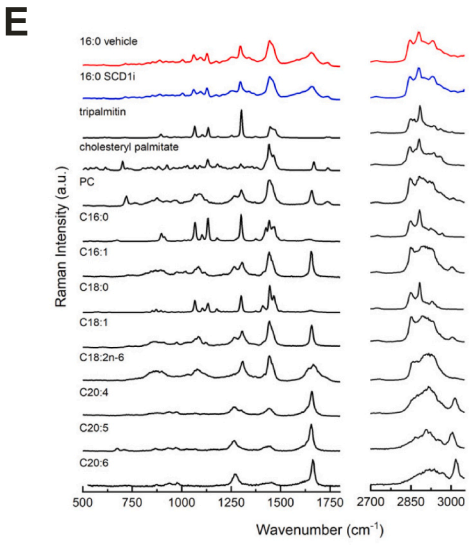


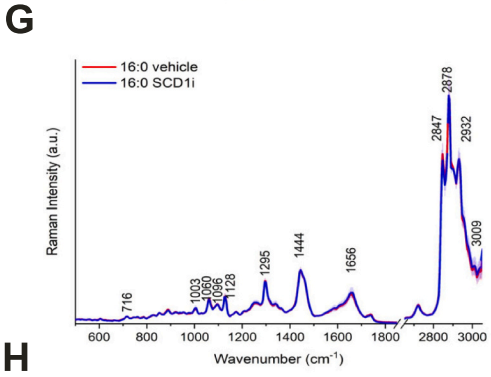


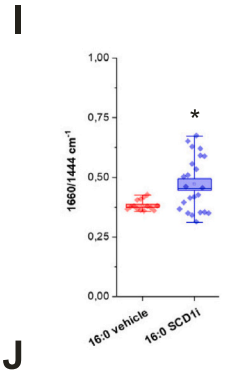


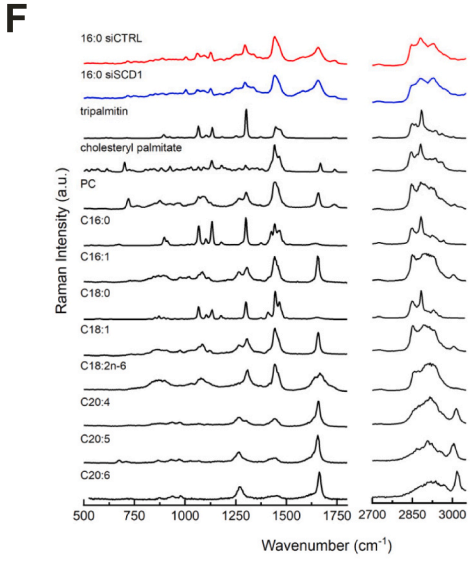


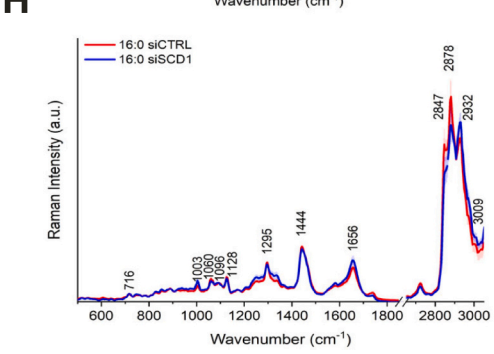


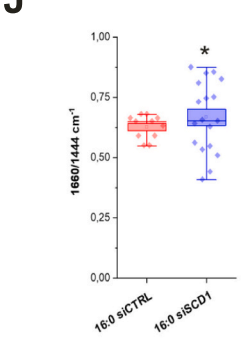


*(caption on next page)*

**Fig. 3.** Downregulation of SCD1 alters compactness, stiffness, and biophysical status of LDs in INS-1E cells after SCD1 inhibition with A939572 (SCD1i) and palmitate (16:0) treatment. Heat-mapped distributions of general polarization (A) and short-wavelength anisotropy corresponding to the ordered lipid phase (B) are represented as 1/99 (circles), 5/95 (whiskers), 25/75 (boxes) percentiles and median values. Statistical differences between distributions were quantified with the Mann-Whitney test (C, D). The data are expressed as the mean ± SD of three independent experiments. $^{*}p < 0.05$, vs. vehicle; $^{\#}p < 0.05$, vs. 16:0 vehicle; $^{\&}p < 0.05$, vs. SCD1i. Comparison of Raman spectra from the LD groups with the spectra of analytical standards of selected saturated and unsaturated FAs or selected lipid species (E, F). Raman spectra of lipid droplets were averaged over all measured INS-1E cells after treatment with the SCD1 inhibitor (G) or genetic deprivation by siRNA against SCD1 (H), followed by co-supplementation with 16:0. Next, the ratio of 1660/1444 $cm^{-1}$ bands was evaluated as the degree of unsaturation (I, J). The Raman measurements were calculated from at least 20 cells per experimental group of three independent imaging experiments. $^{*}p < 0.05$, vs. vehicle/siCTRL.

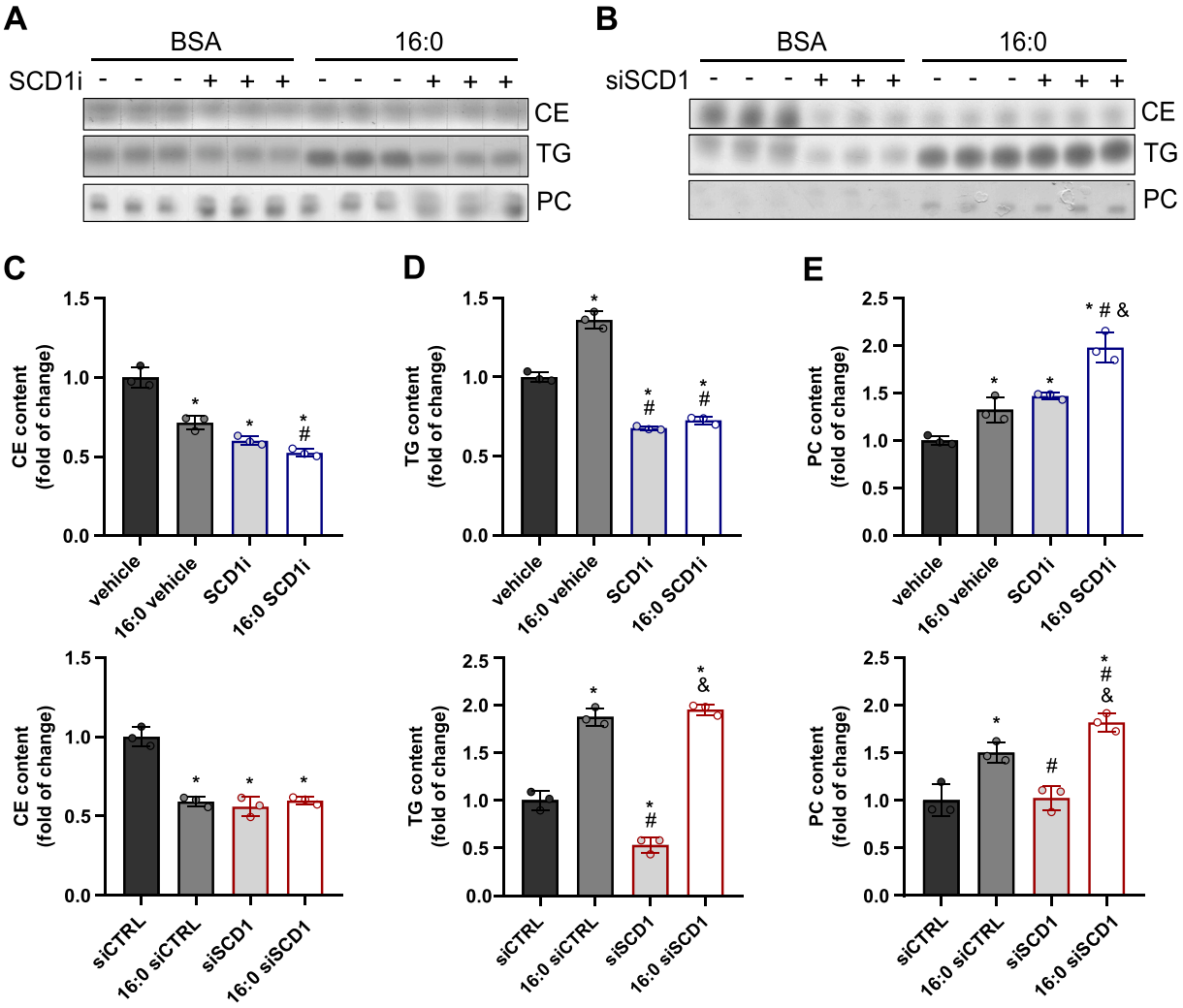


**Fig. 4.** Depletion of the enzymatic activity of SCD1 affects the lipid profile of LDs. Lipid extracts from isolated LDs after SCD1 inhibition or silencing and 16:0 incubation were resolved and analyzed by TLC (A, B). (C–E) Mean ± SD of the spot intensity ratio of cholesteryl esters (CE) (C), triglycerides (TG) (D), and phosphatidylcholine (PC) (E) ($n = 3$). $^{*}p < 0.05$, vs. vehicle/siCTRL; $^{\#}p < 0.05$; vs. 16:0 vehicle/16:0 siCTRL; $^{\&}p < 0.05$, vs. SCD1i/siSCD1.

both SCD1 activity and expression enhanced the elevating effect of palmitate treatment on the abundance of CCTα in INS-1E cells by an average of 30 %. Reciprocally, the content of LPCAT remodeling pathway effectors substantially decreased in the aforementioned experimental groups, suggesting that the Kennedy pathway was favored over Lands' cycle in handling LD-associated PC abundance and composition.

We next determined whether alterations of the PC metabolism-associated proteins and FA composition of the PC mantle affect the distribution or identity of LD-residing proteins. We isolated LDs from SCD1-deficient INS-1E cells after 16 h in BSA or palmitate-supplemented RPMI and then examined the LD-associated proteins by sodium dodecyl sulfate-polyacrylamide gel electrophoresis (SDS-PAGE). Both the pharmacological and genetic depletion of SCD1 with simultaneous palmitate treatment enriched the LD association with effectors of lipolysis, such as hormone-sensitive lipase (HSL), adipose triglyceride lipase (ATGL), and 1-acylglycerol-3-phosphate *O*-acyltransferase (ABHD5), compared with the LD fraction from cells that were incubated with 16:0 itself (Fig. 6C and D). Similarly, ACSL3, PLIN3, and CCTα proteins were detectable in LDs that were purified from palmitate-treated cells and further increased upon parallel SCD1 inhibition or downregulation with siRNA against SCD1. Notably, significant contamination in the LD fractions was excluded by the absence of subcellular localization marker proteins Rab11 and glyceraldehyde 3-phosphate dehydrogenase (GAPDH) from all experimental groups (Fig. 6C and D). Overall, our data indicate that SCD1 mediates local lipid biosynthesis and remodeling in LDs by altering the abundance of proteins at the surface, in turn affecting LD size and its biochemical structure.

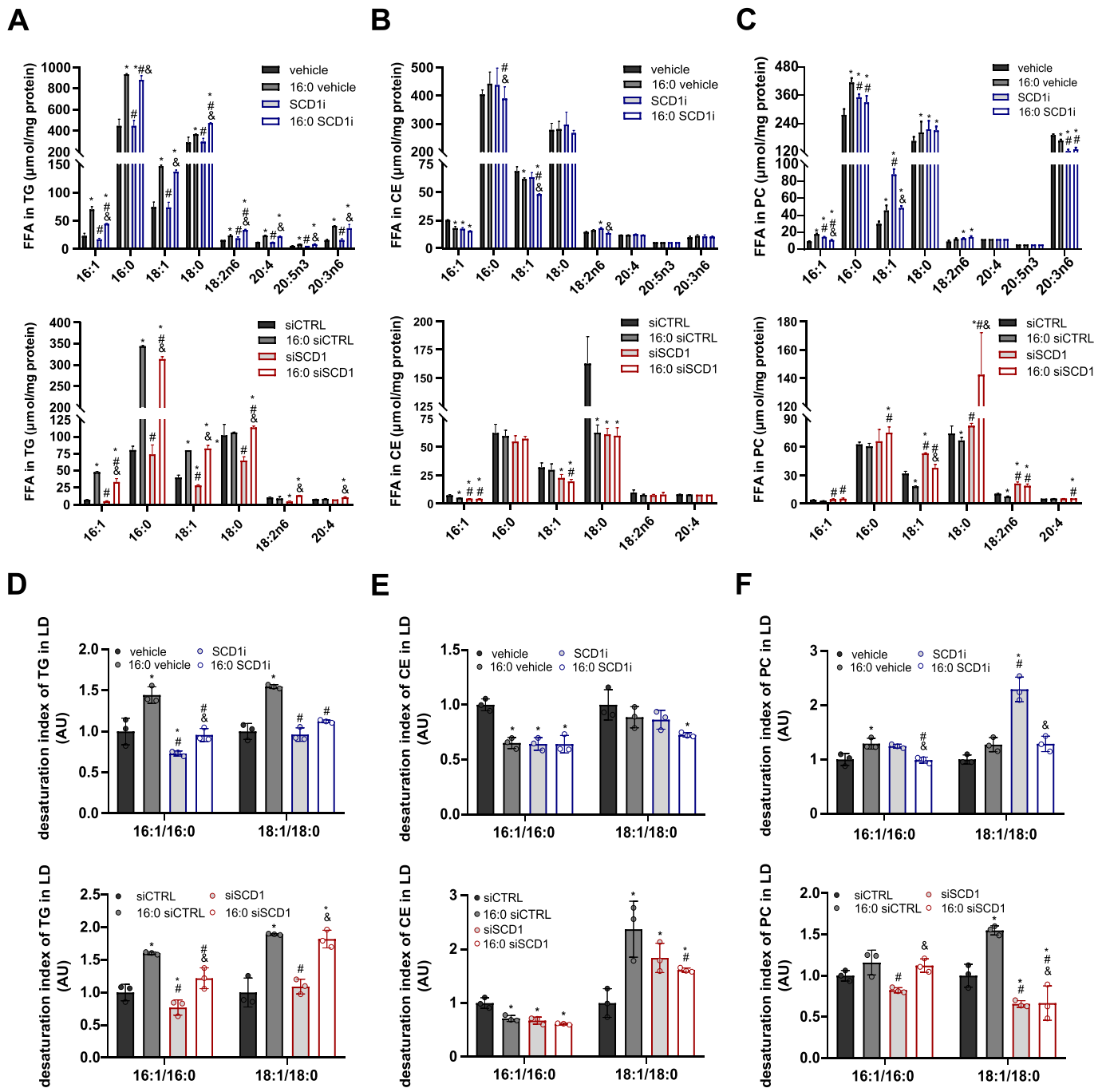


**Fig. 5.** Inhibition of the enzymatic activity of SCD1 affects fatty acid content and saturation status of lipid droplets. Lipid droplets were freshly isolated from INS-1E cells that were incubated with palmitic acid and co-treated with the SCD1 inhibitor A939572 (SCD1i) or siSCD1. The fatty acid composition of TG (A), CE (B), and PC (C) pools was assessed by GC–MS, and their relative changes were normalized to total cellular protein. Next, desaturation status was quantified for separated TG (D), CE (E), and PC (F) as the product-to-substrate ratio (16:1/16:0 and 18:1/18:0). The data are expressed as the mean ± SD of three independent experiments. $^{*}p < 0.05$, vs. vehicle/siCTRL; $^{\#}p < 0.05$, vs. 16:0 vehicle/16:0 siCTRL; $^{\&}p < 0.05$, vs. SCD1i/siSCD1.

### *3.7. Downregulation of SCD1 increases susceptibility to lipotoxicity in murine pancreatic islets*

The pancreas possesses a limited capacity to store lipids and β-cells are highly sensitive to lipid-induced stress [52,53]. To further elucidate the molecular mechanism of SCD1 deprivation on the failure of lipid depots handling, we analyzed islets that were isolated from SCD1$^{-/-}$ mice and wildtype (WT) littermates that were fed a HF diet for 6 weeks. The quantification of Oil Red O staining on pancreatic sections demonstrated that SCD1 deficiency decreased the accumulation of intracellular TGs by over 25 % and 16 % in tissue after a standard laboratory chow diet and a HF diet compared with sections from HF diet-fed control animals, respectively (Fig. 7A). We then analyzed isolated islets by GC–MS to verify the impact of SCD1 deficiency on FA content in selected lipid classes. The effect that we observed during Oil Red O staining was reflected by lower levels of TG total lipids by 73 % and 71 % in islets from SCD1$^{-/-}$ mice that were fed standard laboratory chow and the HF diet, respectively (Fig. 7B). The abundance of CE total lipids also tended to decrease but not significantly (Fig. 7C). However, compared with WT chow-fed mice, the total lipid content in the PC fraction

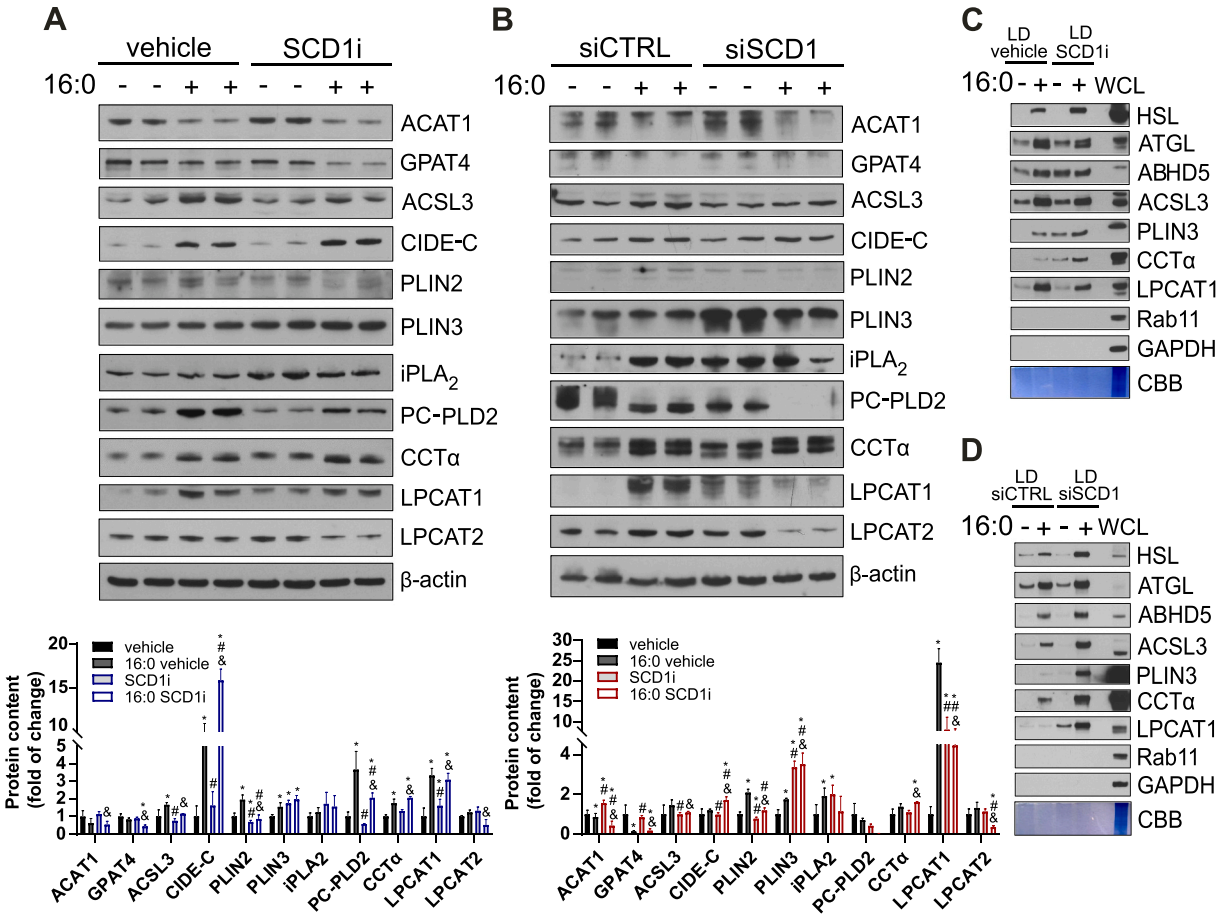


**Fig. 6.** Lipid droplet coating is affected by SCD1 through altered abundance of the proteins involved in PC synthesis and remodeling. (A, B) Western blot analysis of protein levels of ACAT1, GPAT4, ACSL3, CIDE-C, PLIN2, PLIN3, iPLA$_2$, PC-PLD2, CCTα, LPCAT1, and LPCAT2 in INS-1E cells that were subjected to treatment with SCD1 inhibitor A939572 (SCD1i) or siRNA against SCD1 (siSCD1) and palmitic acid (16:0). Levels of proteins were then normalized to β-actin and the vehicle/siCTRL controls. The data are expressed as the mean ± SD of three independent experiments. $^{*}p < 0.05$, vs. vehicle/siCTRL; $^{\#}p < 0.05$, vs. 16:0 vehicle/16:0 siCTRL; $^{\&}p < 0.05$, vs. SCD1i/siSCD1. (C, D) The immunoblotting results showed that SCD1 deficiency affected protein levels of HSL, ATGL, ABHD5, ACSL3, PLIN3, CCTα, and LPCAT1 at the LD surface. Rab11 (an endosome marker) and GAPDH (a cytosol marker) proteins were not enriched in LD fractions that were isolated from INS-1E cells. Minimum three independent isolations of the LD fractions were performed. Coomassie Brilliant Blue G-250 Dye (CBB) was used as a loading control. A whole cell lysate (WCL) sample from INS-1E cells was applied as a correct protein size indicator for each antibody.

significantly increased by 54 % and 67 % in islets from WT and SCD1$^{-/-}$ rodents on the HF diet, respectively (Fig. 7D). As expected, the TG fraction of murine islets from HF diet-maintained WT animals showed an accumulation of saturated 16:0 and 18:0 moieties and an increase in 16:1, 18:1, 18:2n−6, 20:4n−6, and 20:3n−6 FAs. *SCD1* knockdown in islets significantly decreased levels of the aforementioned FAs in TGs compared with WT littermates, independent of the implemented diet (Fig. 7E). Moreover, significant decreases in 16:0, 16:1, and 18:0 FA composition were detected in the CE fraction in the SCD1-deficient islet groups (Fig. 7F). The alterations that were observed in SCD1 desaturase activity between all groups for TG did not reach the level of significance compared with WT chow islets, but we detected reductions of the desaturation index (with a higher preference for 16:0 substrate) in CE and PC content (Supplementary Fig. 3A, B, and C). Accordingly, PC from islets from SCD1$^{-/-}$ HF-fed animals comprised more 18:1, 18:2n−6, 20:4, and 20:5n−3 FAs compared with the PC fraction from islets from control animals and SCD1$^{-/-}$ chow mice (Fig. 7G). This effect was followed by significantly higher levels of overall PUFAs in PC and ELOVL6 and Δ5/6 activities in PC in the aforementioned experimental group (Supplementary Fig. 3D, E, and F).

We next examined the expression of key genes that are related to the biosynthesis, formation, and growth of LDs. Relative to the WT chow control group, we observed significantly higher mRNA levels of *Nem1*, *Snx14*, *Seipin*, *Vps13c*, *Fsp27*, *Gpat4*, *Dgat2*, *Soat1*, and *Acsl3* in WT HF islets (Fig. 7H). SCD1 deficiency was associated with a decrease in the expression of these genes in islets from chow- and more markedly from HF-fed mice compared with WT HF islets.

To verify whether SCD1 deficiency affects LD architecture in murine islets, we evaluated the expression levels of key proteins that are involved in LD-associated protein coating and PC synthesis. Levels of PLIN2 and PLIN5 significantly increased in pancreatic islets from HF-fed mice, but this effect was lowered by SCD1 downregulation. The reciprocal outcome was noted for PLIN3 (Fig. 7I). Furthermore, SCD1 deprivation increased CCTα protein levels >80 % and 50 % in chow and HF islets compared with WT HF islets, respectively. LPCAT1 abundance decreased >80 % in SCD1$^{-/-}$ pancreatic islets, regardless of the type of diet (Fig. 7I). Compared with pancreatic islets from chow-fed WT animals, SCD1-deficient islets had lower mRNA expression of *Pld2* and a higher amount of *Pla2g6* transcript, both of which are crucial genes that are involved in PC synthesis and stability, suggesting that LDs may also serve as a major target for PC turnover in lipid-challenged islets (Fig. 7H). Collectively, these results paralleled our observations from the in vitro model of palmitate-treated INS-1E cells with deficient SCD1 activity and supported the notion that lowering the presence of SCD1 might lead to deficits in LD production and a failure of their metabolic handling in murine pancreatic islets that are subjected to lipid overload.

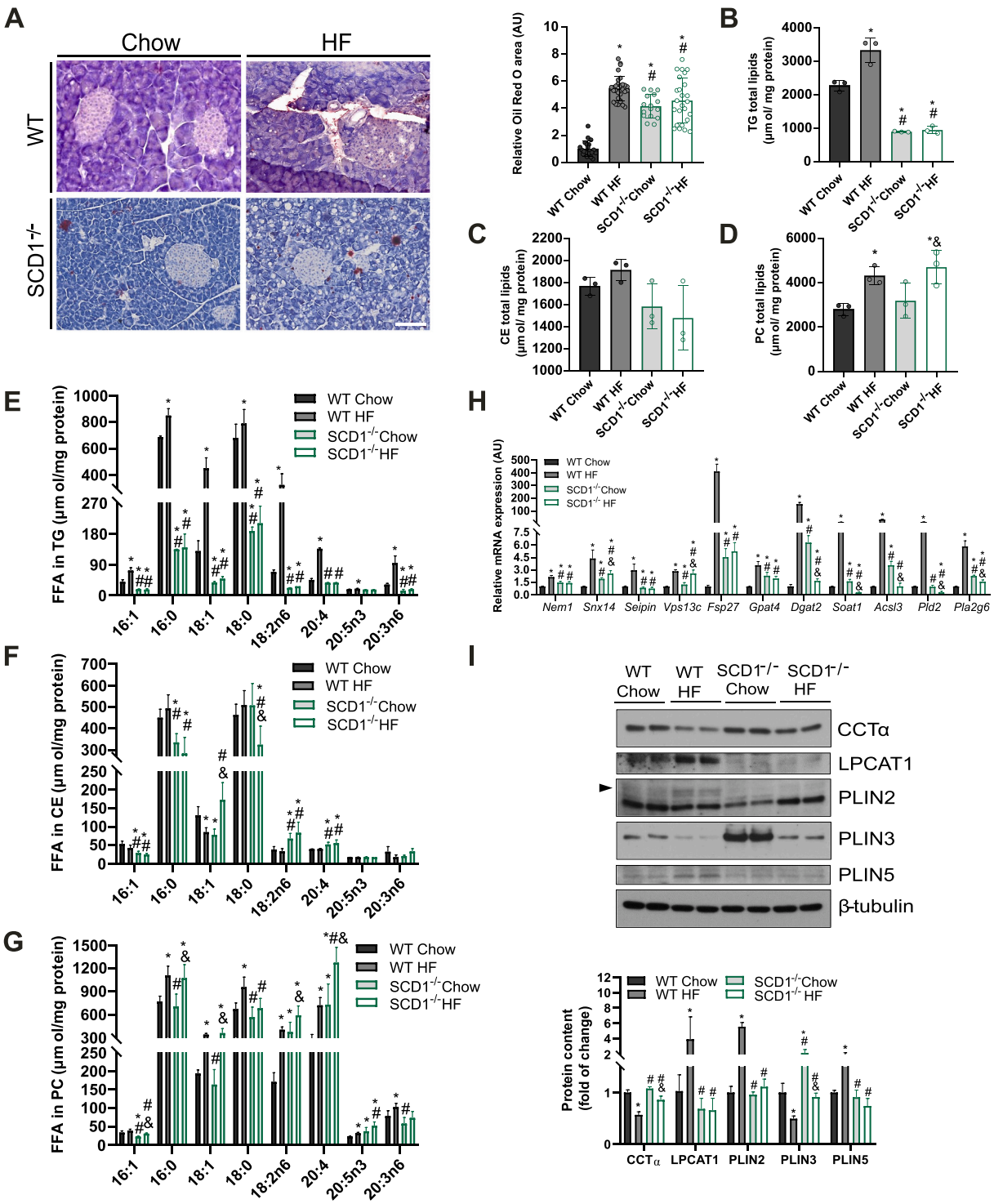


**Fig. 7.** SCD1 deficiency modulates lipid accumulation, content, and handling in murine pancreatic islets. (A) Oil red O staining of lipid depots was quantified in pancreatic sections from wildtype and SCD1$^{-/-}$ mice that were maintained either on chow or a high-fat diet. A representative section for each experimental group is shown ($n \geq 16$). Scale bar = 50 µm. Isolated islets were also subjected to GC–MS analysis, and total lipids of TG (B), CE (C), and PC (D) and the fatty acid composition of TG (E), CE (F), and PC (G) were determined. Relative changes in lipid profiles were normalized to total cellular protein. Subsequently, mRNA expression levels of genes that are involved in the synthesis, formation, and maturation of lipid droplets were evaluated by qRT-PCR in islet extracts (H). The results were normalized to *Rps17*. Levels of proteins that are involved in PC metabolism (CCTα, LPCAT1) and LD coating (PLIN2, PLIN3, PLIN5) were measured in islet extracts by Western blot and then normalized to β-tubulin and the WT chow control (I). Data in A-I are expressed as the mean ± SD of three independent experiments. $^{*}p < 0.05$, vs. WT Chow; $^{\#}p < 0.05$, vs. WT HF; $^{\&}p < 0.05$, vs. SCD1$^{-/-}$ chow.

## 4. Discussion

Obesity and disturbances in the regulation of lipid metabolism are well established risk factors for the development of T2D [4,11,37,52–54]. Non-adipose tissues have a limited capacity to store surplus lipids. Chronic fuel surfeit restrains β-cells from a flawless compensatory response, resulting in glucose intolerance and further islet deterioration [54,55]. Notably, SCD1 remains an important control point of secretory capacity and function in lipid-laden pancreatic β-cells [18,20,21,56]. Our results indicate a novel mechanism of the SCD1-mediated regulation of LD structure and content in rodent pancreatic β-cells. Here, we found that SCD1 deficiency significantly altered the size and amount of LD in parallel with changes in saturation status within core lipids and the composition of FAs of the phospholipid coat. Furthermore, these rearrangements were corroborated by differences in the abundance of LD-associated proteins and compactness and lipid order inside LDs.

Unsurprisingly, ectopic lipid deposition in pancreatic islets triggers widespread tissue malfunction and damage. The degree of islet susceptibility to lipid insult is determined by the chemical structure of FFAs, both their saturation status and carbon chain length [52,57]. Overall, the SCD1-produced MUFAs influence the composition and fluidity of intracellular membrane phospholipids and act as substrates for LDs in various tissues, including pancreatic islets [58,59]. In fact, LDs were enriched in rodent β-cell lines, islet β-cells from donors with T2D, and islet-like β-cells that were generated from human embryonic stem cell-derived β-cell clusters [17,59,60]. Human islets that were transplanted into immunodeficient mice accumulate LDs in β-cells in response to a HF diet [14]. Intriguingly, the long-chain unsaturated fatty acids were able to antagonize palmitotoxicity during co-incubation in RINm5F and INS-1E cells; however, no correlation between the ability of LD formation and protective potency was confirmed [6]. Furthermore, the increase in triglyceride pool in both rat and human dispersed β-cells under nutrient overload was associated with β-cell demise [7].

Genetic inhibition and pharmacological inhibition of the SCD1 enzyme drive a decrease in survival and dysfunction in multiple human and rodent β-cell models [12,18,60–65]. Inhibition of the enzymatic activity of SCD1 led to an aberrant autophagy outcome, perturbations in cellular membrane integrity, and β-cell demise in INS-1E cells [20]. The loss of *SCD1* in leptin-deficient obese BTBR mice resulted in glucose intolerance and accelerated progression to severe diabetes, whereas a subpool of β-cells exhibited signs of SFA-induced lipotoxicity [66]. Individuals with mutations of the seipin gene had higher proportions of SFA in their lipids, suggesting a decrease in SCD activity and a simultaneous decline in the size and amount of LDs [67]. Nevertheless, the exact molecular role of SCD1 in LD formation awaits further clarification. To investigate these mechanisms, we used INS-1E cells whose activity or expression of SCD1 was inhibited. We further validated our data in pancreatic islets from SCD1$^{-/-}$ mice. We observed lower FFA partitioning into complex neutral lipids upon SCD1 deprivation, a phenomenon that was also observed in goat mammary epithelial cells and porcine embryos [27,68]. Moreover, our results in the INS-1E β-cell line are consistent with studies in induced renal epithelial cells, primary hepatocytes and HepG2 cells which demonstrated that SCD1 deficiency was associated with a lower number, diameter, and size of LDs [28,29,69]. Similarly, SCD-deficient *fat-6;fat-7* mutant nematodes exhibited a reduction of fat storage and had fewer and smaller LDs than their wildtype littermates [30]. In fact, in our studies, pharmacological or genetic SCD1 deprivation led to the preferential growth of droplets with an average 10 % smaller diameter compared with respective palmitate-treated control cells. To our knowledge, this is the first comprehensive analysis of the SCD1-mediated effect on LD formation in pancreatic INS-1E β-cells and murine islets.

The causes for this metabolic decline might involve an inability to accumulate neutral lipids into LDs. We further determined biochemical alterations of LDs by measuring LD packing density with the fluorescent PA probe, the GP value of which was used to evaluate LD inner condensation [33,39]. The GP values were lower in LDs that accumulated in cells with low SCD1 activity and co-supplemented with 16:0 than in LDs after stimulation with palmitate alone, leading us to conclude that the inside of the former LDs was more compact, ordered, and stiff than the latter LDs. A more detailed assessment of the biochemical composition of LDs was also supported by the Raman-based approach. The utility of linear Raman imaging spectroscopy to directly monitor LD structure and dynamics while exposed to various FA stimuli was previously successfully applied in hepatocytes and endothelial cells [40,70,71]; to date, it has not been studied in the context of β-cells. The Raman signatures of LDs after in vitro incubation with 16:0 typically resembled TG and CE with regard to spectral characteristics, confirming the uptake and esterification of palmitate into LD structures. Moreover, our results showed that under conditions of SCD1 deficiency, palmitate-induced LDs included significantly higher intensities of unsaturated lipid moiety bands than LDs originating from treatment with palmitic acid alone. We also observed spectral signatures of choline-containing lipids and two amid bands in all experimental groups. Their appearance in a class of LDs can be expected because of the protein impact on the PL mantle at the LD surface [72].

The amounts of the LD surface monolayer and core neutral lipid molecules directly depend on each other [73]. Our GC–MS estimation of the content of lipids that comprised INS-1E LDs provided more detailed data on neutral lipid enrichment that was obtained from the imaging techniques. Indeed, under conditions of SCD1 deprivation, we found a decrease in TG and CE accumulation (i.e., lipid classes that establish the LD core). The high compactness of the neutral lipid core was associated with alterations of desaturation status. Interestingly, the impact of high 16:0 levels on the PL lipidome in INS-1E cells revealed profound changes in the abundance and distribution of FAs in PC [20,74]. Phosphatidylcholine is the most representative constituent of the LD monolayer; thus, it remains critically important for LD stability [75–77]. Phosphatidylcholine shields the underlying hydrophobic lipid core and acts as a surfactant to prevent LD coalescence [75]. Our results indicated that the effect of enzymatic SCD1 depletion on LD size and expansion does not derive exclusively from a decrease in the fraction of accumulated TG and CE, but we also observed the upregulation of PC synthesis and abundance of LD-associated PC. Interestingly, recent studies indicated a direct relationship between high PC levels or FA composition of the surface LD monolayer and the size of LDs, especially in *Drosophila* S2 cells, nematodes, and differentiating 3T3-L1 adipocytes [30,75,78]. Unsaturated fatty acids in PC of the LD mantle and artificial emulsions are engaged in the generation of smaller and less stable LDs [77]. The distribution of MUFAs and PUFAs within the LD monolayer influences its fluidity and biophysical properties, including thickness and order in acyl chains [77–80]. Therefore, the decrease in LD size was expected to also be related to alterations of FA composition of PC in the LD monolayer. A closer examination of the lipid profile of LD-associated PC composition revealed a significant increase in unsaturated 18:1 and 18:2n−6 moieties in PC of LDs from INS-1E cells after the combination of palmitate treatment and SCD1 inhibition or transient silencing with siSCD1. Likewise, higher proportions of 18:2n−6, 20:4, and 20:5n−3 FAs were also confirmed in pancreatic islets from SCD1$^{-/-}$ HF-fed animals compared with the PC fraction from islets from control animals and SCD1$^{-/-}$ chow mice. The high proportion of 18:2n−6 and 20:4n−6 PUFAs in pancreatic PL suggests their importance for membrane fluidity and function [81], which is consistent with our speculation. Similarly, increases in the abundance of 18:2n−6 and 20:4n−6 FAs in the PL fraction of HeLa cells under conditions of SCD1 deficiency and in PC from the liver from SCD1$^{-/-}$ mice were observed, respectively [82,83]. On the contrary, the population of LD-associated PC species enriched in single or two monounsaturated acyl chains in sn−1 and/or sn−2 positions was reported as the extremely rare in HepG2 cells whereas the levels of 16:1n−7 and 18:1n−7 in the PC of the LDs in 3T3-L1 adipocytes increased during the differentiation likely due to elevated SCD1

expression [76,78]. It is also conceivable that SCD1-derived MUFAs in the PC of the LDs are indispensable to facilitate the incorporation of SFAs into TGs, enhance the formation of bigger LDs, and thus make β-cells and pancreatic islets less susceptible to palmitate toxicity. Furthermore, the shape of a PC molecule and its area at the lipid-water interface are influenced by acyl chain unsaturation [84]. Unsaturated fatty acyl chains in PC can drive lipid-packing defects that compromise monolayer curvature, fluidity, fusion abilities, and the final pool of associated proteins [25,73].

Finally, we aimed to confirm whether changes in PC content affect the repertoire of LD-linked proteins. Arguably, the composition of perilipins at the LD surface is also considered a factor that determines LD size [49]. PLIN3 was reported to attach to the surface of small LDs with unsaturated FA moieties [51]. In addition, the functional compensation activity of PLIN3 for a reduced abundance of PLIN2 was also observed in several studies [49,84]. The nonbinding PLIN2/PLIN3-enriched LD fraction in murine adipocytes contained a less rigid and well-supplied in unsaturated FA reservoirs monolayer membrane [85]. This is consistent with our observation, in which we detected higher levels of PLIN3 but reduced abundance of PLIN2 under conditions of SCD1 deprivation in pancreatic β-cells and islets. Another possible explanation involves enzymes that are involved in PC synthesis. Phosphatidylcholine is mainly generated through the Kennedy pathway. Once formed, the FA composition of PC can be remodeled by sequential deacylation (by phospholipases) and reacylation (by LPCAT) via the Lands cycle [86]. Enzymes that are required for both networks relocalize at the surface of LDs; thus, PC can be synthesized and modified locally [47,87]. Deficiencies of both SCD1 activity and expression enhanced the elevating effect of palmitate treatment on the abundance of CCT1α in INS-1E cells, at the LD surface, and in murine SCD1$^{-/-}$ islets. This observation was in line with greater CCT1 activity in the PC fraction in the liver from SCD1$^{-/-}$ mice [83]. CCT1 catalyzes the rate-limiting step of PC synthesis and acts as a biosensor for PC deficits on expanding LDs [75]. This result was complementary to a reduction of PC-PLD2 abundance and substantially lower content of the remodeling pathway effectors LPCAT1 and LPCAT2 that mediate rearrangements of unsaturated FA moieties at the sn−2 position. Notably, LPCAT1 utilizes 18:2-acyl-CoA, and LPCAT2 utilizes 20:4-CoA as the best donor [88]. The interference of Kennedy and Lands networks is important for handling LD-associated PC abundance and composition, and reflects LD size in human hepatoma cell lines [89]. LPCAT-mediated PC synthesis on LDs requires the presence of long chain acyl-CoA and lysophosphatidylcholine as substrates for effective membrane lipid remodeling [87]. Here, we detected a significant decrease in ACSL3 protein content but an increase in iPLA$_2$ levels in INS-1E cells with SCD1 deficiency. Thus, in SCD1-depleted cells, we might observe a lack of compensation for the exchange in PC PUFA composition through an incomplete remodeling pathway [82]. In fact, the high availability of 18:2n−6 might lead to the observed upregulation of 20:4n−6 by activities of SCD1 co-working enzymes (e.g., Δ5/Δ6 desaturases and ELOVL5) in order to eliminate this unstable condition and explain the presence of unsaturated FA Raman features when SCD1 activity is diminished. Alternatively, the FAs can be derived from other membrane compartments since LDs form inter-organelle contacts, which are thought to facilitate flawless trafficking of FAs and prevent lipotoxicity [72]. The remodeling of ER-associated PC and polyunsaturated phospholipids decreased tension, controlled FA handover to LDs, and preferentially enabled specific neutral lipids' budding in small LDs [24].

On the other hand, cylinder-like PC decreases surface tension and stabilizes the LD surface, thus preventing their coalescence [75,77]. Regardless of the high abundance of PC (but not with preferential FA composition) and increase in the abundance of CIDE-C, INS-1E and pancreatic islet cells face a critical mass in lipid storage at some point under conditions of SCD1 deprivation. In accordance with this possibility, SCD1 overexpression decreased LD enrichment with CCT1 and restored large LDs in INS-1E cells (Supplementary Fig. 4) and goat mammary epithelial cells [27]. Low levels of CCT1 would allow for the generation of supersized lipolysis-resistant LDs [75]. Alternatively, the effective neutralization of lipid-induced stress is mediated by LD breakdown by catabolic lipolysis or lipophagy processes. During lipolysis, stored TGs are broken down by LD-associated lipases [90]. The chronic stimulation of lipolysis resulted in large-to-small LD fragmentation in adipocytes [76]. Apart from lower levels of TG and CE in the LD core, we observed the enrichment of HSL, ATGL, and ABHD5 (effectors of lipolysis) at the LD surface upon SCD1 deprivation, suggesting that this process remains functional. Moreover, we previously observed a substantial increase in DG turnover under conditions of SCD1 deficiency, which can also serve as a substrate for PC production [20,77]. In turn, during lipophagy, autophagosomes engulf LDs and fuse with lysosomes to be degraded by lysosomal hydrolases [90]. We recently showed that the inhibition of SCD1 activity affects autophagosome-lysosome fusion by perturbations in cellular membrane integrity and FA composition, thus leading to β-cell demise [20]. Given the pivotal significance of autophagy for the proper architecture and flawless function of pancreatic β-cells [91], LD breakdown under conditions of SCD1 deficiency may be incomplete, and pancreatic β-cells may eventually reach an LD saturation threshold. However, further studies are necessary to support this possibility.

Excessive nutritional load that derives from circulating toxic FFAs and an increase in the accumulation of local pancreatic fat triggers structural and functional changes in T2D-affected islets [11,15]. Hence, the ability of β-cells to regulate the traffic of lipids into and out of LDs appears to be a reasonable strategy to mitigate lipotoxicity outcomes [15]. The preservation of β-cell mass and function remains a main goal of T2D management under stressful conditions of lipid insult. Our results revealed an unexpected cellular route for regulating the size and number of LDs in INS-1E cells and murine pancreatic islets under conditions of lipid surplus, reassuring SCD1 deficiency as the main brake on palmitate toxicity and suggesting that SCD1 full function is yet more complex than currently considered. By investigating the network of LD biogenesis, expansion, and metabolism, we identify a link between the step of Δ9 desaturation in FA biosynthesis and LD homeostasis. We propose that SCD1 activity controls LD size and morphology, likely by affecting surface PC FA content and the capacity for its remodeling. Subsequently, the proper composition of the LD phospholipid monolayer is required for efficient LD metabolism, expansion, and disposal [73], in which the aforementioned changes determine the pool of LD-associated protein components that are responsible for these processes (Fig. 8). Ultimately, the beneficial effects of systemic SCD1 inhibition on adiposity may occur at the expense of β-cells, warning against the clinical use of SCD1 inhibition in these crucial cells [92]. Lipid droplets can be successfully applied as stable and biocompatible tools that help effectively resist cellular stress and alleviate lipotoxicity [93]. The potency of affecting LDs' number, size, or lipid composition holds promise for novel therapeutic interventions for T2D treatment.

Supplementary data to this article can be found online at https://doi.org/10.1016/j.bbadis.2023.166711.

## CRediT authorship contribution statement

**Justyna Janikiewicz:** Writing – original draft, Investigation, Resources, Formal analysis, Visualization, Conceptualization, Supervision, Project administration, Funding acquisition. **Aneta M. Dobosz:** Writing – review & editing, Investigation, Resources, Formal analysis, Visualization. **Katarzyna Majzner:** Writing – review & editing, Investigation, Resources, Formal analysis, Visualization. **Tytus Bernas:** Writing – review & editing, Investigation, Resources, Formal analysis, Visualization. **Agnieszka Dobrzyn:** Writing – original draft, Conceptualization.

## Declaration of competing interest

The authors declare that they have no known competing financial interests or personal relationships that could have appeared to influence

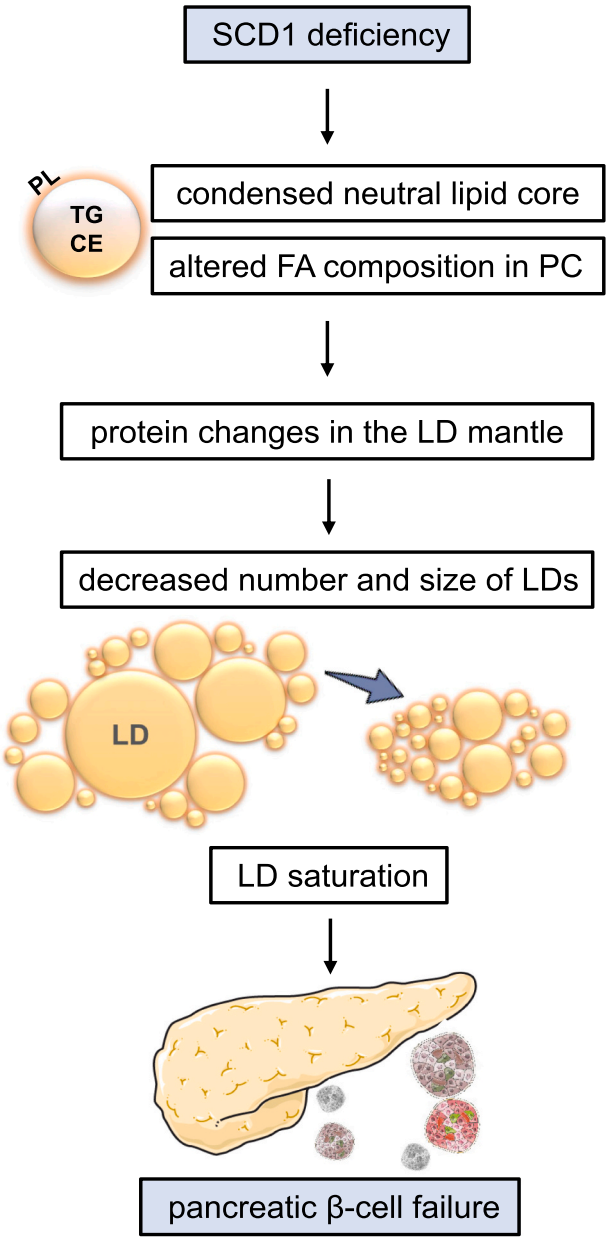


**Fig. 8.** Suggested mechanism of the effect of SCD1 deprivation on the regulation of LD morphology, abundance, composition, and metabolism. The down-regulation of SCD1 during the lipid oversupply of pancreatic β-cells results in lower LD accumulation. Because of inner LD rearrangements (i.e., more compact and stiff neutral lipid core) and external alterations of the phospholipid monolayer (PC fatty acid composition), a repertoire of proteins that decorate the LD surface is affected. Consequently, an aberrant interactome and SCD1 deficiency lead to droplets with a smaller diameter and lower overall fat storage capacity in the cytoplasm. This simplified model may explain the reason for β-cell demise when the LD saturation threshold is reached under lipotoxic conditions.

the work reported in this paper.

## Data availability

Data will be made available on request.

## Acknowledgements

The authors are grateful to Malgorzata Calka-Kreza and Artur Wolny for excellent assistance with the microscopic analysis, Paulina Pawelec for technical support and Michael Arends for proofreading the manuscript. Servier Medical Art by Servier, licensed under a Creative Commons Attribution 3.0 Unported License, was the source of graphical elements in Fig. 8. This work was supported by a grant from the National Science Centre, Poland (no. UMO-2015/19/D/NZ4/03705 to J.J.).

## References

[1] Z.W. Man, M. Zhu, Y. Noma, K. Toide, T. Sato, Y. Asahi, et al., Impaired beta-cell function and deposition of fat droplets in the pancreas as a consequence of hypertriglyceridemia in OLETF rat, a model of spontaneous NIDDM, Diabetes 46 (11) (1997) 1718–1724.

[2] M. Suleiman, L. Marselli, M. Cnop, D.L. Eizirik, C. De Luca, F.R. Femia, et al., The role of beta cell recovery in type 2 diabetes remission, Int. J. Mol. Sci. 23 (13) (2022) 7435.

[3] L. Marselli, J. Thorne, S. Dahiya, D.C. Sgroi, A. Sharma, S. Bonner-Weir, et al., Gene expression profiles of Beta-cell enriched tissue obtained by laser capture microdissection from subjects with type 2 diabetes, PLoS One 5 (7) (2010), e11499.

[4] J. Janikiewicz, K. Hanzelka, K. Kozinski, K. Kolczynska, A. Dobrzyn, Islet β-cell failure in type 2 diabetes-within the network of toxic lipids, Biochem. Biophys. Res. Commun. 460 (3) (2015) 491–496.

[5] L.L. Listenberger, X. Han, S.E. Lewis, S. Cases, R.V. Farese Jr., D.S. Ory, et al., Triglyceride accumulation protects against fatty acid-induced lipotoxicity, Proc. Natl. Acad. Sci. U. S. A. 100 (6) (2003) 3077–3082.

[6] T. Plötz, M. Hartmann, S. Lenzen, M. Elsner, The role of lipid droplet formation in the protection of unsaturated fatty acids against palmitic acid induced lipotoxicity to rat insulin-producing cells, Nutr. Metab. (Lond.) 13 (2016) 16.

[7] S. Vernier, A. Chiu, J. Schober, T. Weber, P. Nguyen, M. Luer, et al., β-Cell metabolic alterations under chronic nutrient overload in rat and human islets, Islets. 4 (6) (2012) 379–392.

[8] T.C. Walther, R.V. Farese Jr., Lipid droplets and cellular lipid metabolism, Annu. Rev. Biochem. 81 (2012) 687–714.

[9] G. Onal, O. Kutlu, D. Gozuacik, Emre S. Dokmeci, Lipid droplets in health and disease, Lipids Health Dis. 16 (1) (2017) 128.

[10] N. Kory, R.V. Farese Jr., T.C. Walther, Targeting fat: mechanisms of protein localization to lipid droplets, Trends Cell Biol. 26 (7) (2016) 535–546.

[11] Y. Imai, R.S. Cousins, S. Liu, B.M. Phelps, J.A. Promes, Connecting pancreatic islet lipid metabolism with insulin secretion and the development of type 2 diabetes, Ann. N. Y. Acad. Sci. 1461 (1) (2020) 53–72.

[12] A.K. Busch, E. Gurisik, D.V. Cordery, M. Sudlow, G.S. Denyer, D.R. Laybutt, et al., Increased fatty acid desaturation and enhanced expression of stearoyl coenzyme A desaturase protects pancreatic beta-cells from lipoapoptosis, Diabetes. 54 (10) (2005) 2917–2924.

[13] H. Wang, P. Maechler, P.A. Antinozzi, L. Herrero, K.A. Hagenfeldt-Johansson, A. Bjorklund, et al., The transcription factor SREBP-1c is instrumental in the development of beta-cell dysfunction, J. Biol. Chem. 278 (19) (2003) 16622–16629.

[14] C. Dai, N.S. Kayton, A. Shostak, G. Poffenberger, H.A. Cyphert, R. Aramandla, et al., Stress-impaired transcription factor expression and insulin secretion in transplanted human islets, J. Clin. Invest. 126 (5) (2016) 1857–1870.

[15] X. Tong, R. Stein, Lipid droplets protect human β-cells from lipotoxicity-induced stress and cell identity changes, Diabetes 70 (11) (2021) 2595–2607.

[16] T. Horii, J. Kozawa, Y. Fujita, S. Kawata, H. Ozawa, C. Ishibashi, et al., Lipid droplet accumulation in β cells in patients with type 2 diabetes is associated with insulin resistance, hyperglycemia and β cell dysfunction involving decreased insulin granules, Front. Endocrinol. (Lausanne) 13 (2022), 996716.

[17] M. Cnop, J.C. Hannaert, A. Hoorens, D.L. Eizirik, D.G. Pipeleers, Inverse relationship between cytotoxicity of free fatty acids in pancreatic islet cells and cellular triglyceride accumulation, Diabetes 50 (8) (2001) 1771–1777.

[18] M. Oshima, S. Pechberty, L. Bellini, S.O. Göpel, M. Campana, C. Rouch, et al., Stearoyl CoA desaturase is a gatekeeper that protects human beta cells against lipotoxicity and maintains their identity, Diabetologia 63 (2) (2020) 395–409.

[19] J.M. Ntambi, M. Miyazaki, Regulation of stearoyl-CoA desaturases and role in metabolism, Prog. Lipid Res. 43 (2) (2004) 91–104.

[20] J. Janikiewicz, K. Hanzelka, A. Dziewulska, K. Kozinski, P. Dobrzyn, T. Bernas, et al., Inhibition of SCD1 impairs palmitate-derived autophagy at the step of autophagosome-lysosome fusion in pancreatic β-cells, J. Lipid Res. 56 (10) (2015) 1901–1911.

[21] A.M. Dobosz, J. Janikiewicz, A.M. Borkowska, A. Dziewulska, E. Lipiec, P. Dobrzyn, et al., Stearoyl-CoA desaturase 1 activity determines the maintenance of DNMT1-mediated DNA methylation patterns in pancreatic β-cells, Int. J. Mol. Sci. 21 (18) (2020) 6844.

[22] C.D. Green, L.K. Olson, Modulation of palmitate-induced endoplasmic reticulum stress and apoptosis in pancreatic β-cells by stearoyl-CoA desaturase and Elovl6, Am. J. Physiol. Endocrinol. Metab. 300 (4) (2011) E640–E649.

[23] K. Thörn, M. Hovsepyan, P. Bergsten, Reduced levels of SCD1 accentuate palmitate-induced stress in insulin-producing β-cells, Lipids Health Dis. 9 (2010) 108.

[24] K. Ben M'barek, D. Ajjaji, A. Chorlay, S. Vanni, L. Forêt, A.R. Thiam, ER membrane phospholipids and surface tension control cellular lipid droplet formation, Dev. Cell 41 (6) (2017) 591–604.e7.

[25] R.K. Lyn, R. Singaravelu, S. Kargman, S. O'Hara, H. Chan, R. Oballa, et al., Stearoyl-CoA desaturase inhibition blocks formation of hepatitis C virus-induced specialized membranes, Sci. Rep. 1 (4) (2014) 4549.
[26] T. Iwai, S. Kume, M. Chin-Kanasaki, S. Kuwagata, H. Araki, N. Takeda, et al., Stearoyl-CoA desaturase-1 protects cells against lipotoxicity-mediated apoptosis in proximal tubular cells, Int. J. Mol. Sci. 17 (11) (2016) 1868.
[27] C. Ren, L. Wang, Y. Fan, R. Jia, G. Zhang, M. Deng, et al., Scd1 contributes to lipid droplets formation in GMEC via transcriptional regulation of Tip47 and Adrp, Eur. J. Lipid Sci. Technol. 120 (2018) 1700238.
[28] M.A. Lounis, K.F. Bergeron, M.S. Burhans, J.M. Ntambi, C. Mounier, Oleate activates SREBP-1 signaling activity in *SCD1*-deficient hepatocytes, Am. J. Physiol. Endocrinol. Metab. 313 (6) (2017) E710–E720.
[29] M.A. Lounis, S. Lalonde, S.A. Rial, K.F. Bergeron, J.C. Ralston, D.M. Mutch, et al., Hepatic BSCL2 (Seipin) deficiency disrupts lipid droplet homeostasis and increases lipid metabolism via SCD1 activity, Lipids. 52 (2) (2017) 129–150.
[30] X. Shi, J. Li, X. Zou, J. Greggain, S.V. Rødkær, N.J. Færgeman, et al., Regulation of lipid droplet size and phospholipid composition by stearoyl-CoA desaturase, J. Lipid Res. 54 (9) (2013) 2504–2514.
[31] M. Miyazaki, W.C. Man, J.M. Ntambi, Targeted disruption of stearoyl-CoA desaturase1 gene in mice causes atrophy of sebaceous and meibomian glands and depletion of wax esters in the eyelid, J. Nutr. 131 (9) (2001) 2260–2268.
[32] D.L. Brasaemle, N.E. Wolins, Isolation of lipid droplets. Methods, in: Current Protocols in Cell Biology, John Wiley & Sons, Inc., 2006, pp. 3.15.1–3.15.12 (Supplement 29, Unit 3.15).
[33] Y. Niko, P. Didier, Y. Mely, G. Konishi, A.S. Klymchenko, Bright and photostable push-pull pyrene dye visualizes lipid order variation between plasma and intracellular membranes, Sci. Rep. 6 (2016) 18870.
[34] J. Brewer, H.S. Thoke, R.P. Stock, L.A. Bagatolli, Enzymatic studies on planar supported membranes using a widefield fluorescence LAURDAN Generalized Polarization imaging approach, Biochim. Biophys. Acta Biomembr. 1859 (5) (2017) 888–895.
[35] K. Majzner, S. Tott, L. Roussille, V. Deckert, S. Chlopicki, M. Baranska, Uptake of fatty acids by a single endothelial cell investigated by Raman spectroscopy supported by AFM, Analyst. 143 (4) (2018) 970–980.
[36] E.G. Bligh, W.J. Dyer, A rapid method of total lipid extraction and purification, Can. J. Biochem. Physiol. 37 (8) (1959) 911–917.
[37] Y.S. Oh, G.D. Bae, D.J. Baek, E.Y. Park, H.S. Jun, Fatty acid-induced lipotoxicity in pancreatic beta-cells during development of type 2 diabetes, Front. Endocrinol. (Lausanne) 9 (2018) 384.
[38] M. Lytrivi, K. Ghaddar, M. Lopes, V. Rosengren, A. Piron, X. Yi, et al., Combined transcriptome and proteome profiling of the pancreatic β-cell response to palmitate unveils key pathways of β-cell lipotoxicity, BMC Genomics 21 (1) (2020) 590.
[39] S. Mazeres, F. Fereidouni, E. Joly, Using spectral decomposition of the signals from laurdan-derived probes to evaluate the physical state of membranes in live cells, F1000Res 6 (2017) 763.
[40] K. Majzner, K. Kochan, N. Kachamakova-Trojanowska, E. Maslak, S. Chlopicki, M. Baranska, Raman imaging providing insights into chemical composition of lipid droplets of different size and origin: in hepatocytes and endothelium, Anal. Chem. 86 (13) (2014) 6666–6674.
[41] C. Beermann, M. Möbius, N. Winterling, J.J. Schmitt, G. Boehm, sn-Position determination of phospholipid-linked fatty acids derived from erythrocytes by liquid chromatography electrospray ionization ion-trap mass spectrometry, Lipids 40 (2) (2005) 211–218.
[42] V.T. Salo, I. Belevich, S. Li, L. Karhinen, H. Vihinen, C. Vigouroux, et al., Seipin regulates ER-lipid droplet contacts and cargo delivery, EMBO J. 35 (24) (2016) 2699–2716.
[43] B.C. Cohen, A. Shamay, N. Argov-Argaman, Regulation of lipid droplet size in mammary epithelial cells by remodeling of membrane lipid composition-a potential mechanism, PLoS One 10 (3) (2015), e0121645.
[44] B.C. Cohen, C. Raz, A. Shamay, N. Argov-Argaman, Lipid droplet fusion in mammary epithelial cells is regulated by phosphatidylethanolamine metabolism, J. Mammary Gland Biol. Neoplasia 22 (4) (2017) 235–249.
[45] D. Hishikawa, T. Hashidate, T. Shimizu, H. Shindou, Diversity and function of membrane glycerophospholipids generated by the remodeling pathway in mammalian cells, J. Lipid Res. 55 (5) (2014) 799–807.
[46] J.Y. Zhang, K.S. Kothapalli, J.T. Brenna, Desaturase and elongase-limiting endogenous long-chain polyunsaturated fatty acid biosynthesis, Curr. Opin. Clin. Nutr. Metab. Care 19 (2) (2016) 103–110.
[47] S. Xu, X. Zhang, P. Liu, Lipid droplet proteins and metabolic diseases, Biochim. Biophys. Acta Mol. basis Dis. 1864 (5 Pt B) (2018) 1968–1983.
[48] K. Bersuker, J.A. Olzmann, Establishing the lipid droplet proteome: mechanisms of lipid droplet protein targeting and degradation, Biochim. Biophys. Acta Mol. Cell Biol. Lipids 1862 (10 Pt B) (2017) 1166–1177.
[49] X. Tong, S. Liu, R. Stein, Y. Imai, Lipid droplets' role in the regulation of β-cell function and β-cell demise in type 2 diabetes, Endocrinology 163 (3) (2022), bqac007.
[51] M. Mirheydari, S.S. Rathnayake, H. Frederick, T. Arhar, E.K. Mann, S. Cocklin, et al., Insertion of perilipin 3 into a glycero(phospho)lipid monolayer depends on lipid headgroup and acyl chain species, J. Lipid Res. 57 (8) (2016) 1465–1476.
[52] M. Lytrivi, A.L. Castell, V. Poitout, M. Cnop, Recent insights into mechanisms of β-cell lipo- and glucolipotoxicity in type 2 diabetes, J. Mol. Biol. 432 (5) (2020) 1514–1534.
[53] D.L. Eizirik, L. Pasquali, M. Cnop, Pancreatic β-cells in type 1 and type 2 diabetes mellitus: different pathways to failure, Nat. Rev. Endocrinol. 16 (7) (2020) 349–362.
[54] M. Prentki, M.L. Peyot, P. Masiello, S.R.M. Madiraju, Nutrient-induced metabolic stress, adaptation, detoxification, and toxicity in the pancreatic β-cell, Diabetes. 69 (3) (2020) 279–290.
[55] E.U. Alejandro, B. Gregg, M. Blandino-Rosano, C. Cras-Méneur, E. Bernal-Mizrachi, Natural history of β-cell adaptation and failure in type 2 diabetes, Mol. Asp. Med. 42 (2015) 19–41.
[56] A.M. ALJohani, D.N. Syed, J.M. Ntambi, Insights into stearoyl-CoA desaturase-1 regulation of systemic metabolism, Trends Endocrinol. Metab. 28 (12) (2017) 831–842.
[57] T. Plötz, A.S. von Hanstein, B. Krümmel, A. Laporte, I. Mehmeti, S. Lenzen, Structure-toxicity relationships of saturated and unsaturated free fatty acids for elucidating the lipotoxic effects in human EndoC-βH1 beta-cells, Biochim. Biophys. Acta Mol. basis Dis. 1865 (11) (2019) 165525.
[58] D. Mauvoisin, C. Mounier, Hormonal and nutritional regulation of SCD1 gene expression, Biochimie 93 (1) (2011) 78–86.
[59] S. Larsson, S. Resjö, M.F. Gomez, P. James, C. Holm, Characterization of the lipid droplet proteome of a clonal insulin-producing β-cell line (INS-1 832/13), J. Proteome Res. 11 (2) (2012) 1264–1273.
[60] R. Lupi, F. Dotta, L. Marselli, S. Del Guerra, M. Masini, C. Santangelo, et al., Prolonged exposure to free fatty acids has cytostatic and pro-apoptotic effects on human pancreatic islets: evidence that beta-cell death is caspase mediated, partially dependent on ceramide pathway, and Bcl-2 regulated, Diabetes 51 (5) (2002) 1437–1442.
[61] K. Maedler, J. Oberholzer, P. Bucher, G.A. Spinas, M.Y. Donath, Monounsaturated fatty acids prevent the deleterious effects of palmitate and high glucose on human pancreatic beta-cell turnover and function, Diabetes 52 (3) (2003) 726–733.
[62] S. Piro, M. Anello, C. Di Pietro, M.N. Lizzio, G. Patanè, A.M. Rabuazzo, et al., Chronic exposure to free fatty acids or high glucose induces apoptosis in rat pancreatic islets: possible role of oxidative stress, Metabolism 51 (10) (2002) 1340–1347.
[63] I. Maestre, J. Jordán, S. Calvo, J.A. Reig, V. Ceña, B. Soria, et al., Mitochondrial dysfunction is involved in apoptosis induced by serum withdrawal and fatty acids in the β-cell line INS-1, Endocrinology 144 (1) (2003) 335–345.
[64] K.H. Hellemans, J.C. Hannaert, B. Denys, K.R. Steffensen, C. Raemdonck, G. A. Martens, et al., Susceptibility of pancreatic beta cells to fatty acids is regulated by LXR/PPARalpha-dependent stearoyl-coenzyme A desaturase, PLoS One 4 (9) (2009), e7266.
[65] K. Thörn, P. Bergsten, Fatty acid-induced oxidation and triglyceride formation is higher in insulin-producing MIN6 cells exposed to oleate compared to palmitate, J. Cell. Biochem. 111 (2) (2010) 497–507.
[66] J.B. Flowers, M.E. Rabaglia, K.L. Schueler, M.T. Flowers, H. Lan, M.P. Keller, et al., Loss of stearoyl-CoA desaturase-1 improves insulin sensitivity in lean mice but worsens diabetes in leptin-deficient obese mice, Diabetes 56 (5) (2007) 1228–1239.
[67] E. Boutet, H. El Mourabit, M. Prot, M. Nemani, E. Khallouf, O. Colard, et al., Seipin deficiency alters fatty acid Delta9 desaturation and lipid droplet formation in Berardinelli-Seip congenital lipodystrophy, Biochimie 91 (6) (2009) 796–803.
[68] D.K. Lee, K.H. Choi, J.Y. Hwang, J.N. Oh, S.H. Kim, C.K. Lee, Stearoyl-coenzyme A desaturase 1 is required for lipid droplet formation in pig embryo, Reproduction 157 (3) (2019) 235–243.
[69] A. Pérez-Martí, S. Ramakrishnan, J. Li, A. Dugourd, M.R. Molenaar, L.R. De La Motte, et al., Reducing lipid bilayer stress by monounsaturated fatty acids protects renal proximal tubules in diabetes, Elife 11 (2022), e74391 (2022 May 12).
[70] K. Czamara, K. Majzner, A. Selmi, M. Baranska, Y. Ozaki, A. Kaczor, Unsaturated lipid bodies as a hallmark of inflammation studied by Raman 2D and 3D microscopy, Sci. Rep. 8 (7) (2017), 40889.
[71] M.Z. Pacia, K. Majzner, K. Czamara, M. Sternak, S. Chlopicki, M. Baranska, Estimation of the content of lipids composing endothelial lipid droplets based on Raman imaging, Biochim. Biophys. Acta Mol. Cell Biol. Lipids 2020 (9) (1865) 158758.
[72] J.A. Olzmann, P. Carvalho, Dynamics and functions of lipid droplets, Nat. Rev. Mol. Cell Biol. 20 (3) (2019) 137–155.
[73] A. Penno, G. Hackenbroich, C. Thiele, Phospholipids and lipid droplets, Biochim. Biophys. Acta 1831 (3) (2013) 589–594.
[74] G. Maulucci, O. Cohen, B. Daniel, C. Ferreri, S. Sasson, The combination of whole cell lipidomics analysis and single cell confocal imaging of fluidity and micropolarity provides insight into stress-induced lipid turnover in subcellular organelles of pancreatic beta cells, Molecules. 24 (20) (2019) 3742.
[75] N. Krahmer, Y. Guo, F. Wilfling, M. Hilger, S. Lingrell, K. Heger, et al., Phosphatidylcholine synthesis for lipid droplet expansion is mediated by localized activation of CTP:phosphocholine cytidylyltransferase, Cell Metab. 14 (4) (2011) 504–515.
[76] K. Tauchi-Sato, S. Ozeki, T. Houjou, R. Taguchi, T. Fujimoto, The surface of lipid droplets is a phospholipid monolayer with a unique fatty acid composition, J. Biol. Chem. 277 (46) (2002) 44507–44512.
[77] K. Arisawa, H. Mitsudome, K. Yoshida, S. Sugimoto, T. Ishikawa, Y. Fujiwara, et al., Saturated fatty acid in the phospholipid monolayer contributes to the formation of large lipid droplets, Biochem. Biophys. Res. Commun. 480 (4) (2016) 641–647.
[78] K. Arisawa, I. Ichi, Y. Yasukawa, Y. Sone, Y. Fujiwara, Changes in the phospholipid fatty acid composition of the lipid droplet during the differentiation of 3T3-L1 adipocytes, J. Biochem. 154 (3) (2013) 281–289.
[79] F. Geltinger, L. Schartel, M. Wiederstein, J. Tevini, E. Aigner, T.K. Felder, et al., Friend or foe: lipid droplets as organelles for protein and lipid storage in cellular stress response, aging and disease, Molecules 25 (21) (2020), 5053.
[80] T. Harayama, T. Shimizu, Roles of polyunsaturated fatty acids, from mediators to membranes, J. Lipid Res. 61 (8) (2020) 1150–1160 (Aug).

[81] K.E. Pinnick, S.C. Collins, C. Londos, D. Gauguier, A. Clark, B.A. Fielding, Pancreatic ectopic fat is characterized by adipocyte infiltration and altered lipid composition, Obesity (Silver Spring) 6 (3) (2008) 522–530.
[82] H. Ariyama, N. Kono, S. Matsuda, T. Inoue, H. Arai, Decrease in membrane phospholipid unsaturation induces unfolded protein response, J. Biol. Chem. 285 (29) (2010) 22027–22035.
[83] A. Dobrzyn, P. Dobrzyn, M. Miyazaki, H. Sampath, K. Chu, J.M. Ntambi, Stearoyl-CoA desaturase 1 deficiency increases CTP:choline cytidylyltransferase translocation into the membrane and enhances phosphatidylcholine synthesis in liver, J. Biol. Chem. 280 (24) (2005) 23356–23362.
[84] C. Sztalryd, M. Bell, X. Lu, P. Mertz, S. Hickenbottom, B.H. Chang, et al., Functional compensation for adipose differentiation-related protein (ADFP) by Tip47 in an ADFP null embryonic cell line, J. Biol. Chem. 281 (45) (2006) 34341–34348.
[85] S.M. Storey, A.L. McIntosh, S. Senthivinayagam, K.C. Moon, B.P. Atshaves, The phospholipid monolayer associated with perilipin-enriched lipid droplets is a highly organized rigid membrane structure, Am. J. Physiol. Endocrinol. Metab. 301 (5) (2011) E991–E1003.
[86] J.E. Vance, D.E. Vance, Phospholipid biosynthesis in mammalian cells, Biochem. Cell Biol. 82 (1) (2004) 113–128.
[87] C. Moessinger, L. Kuerschner, J. Spandl, A. Shevchenko, C. Thiele, Human lysophosphatidylcholine acyltransferases 1 and 2 are located in lipid droplets where they catalyze the formation of phosphatidylcholine, J. Biol. Chem. 286 (24) (2011) 21330–21339.
[88] H. Shindou, T. Shimizu, Acyl-CoA:lysophospholipid acyltransferases, J. Biol. Chem. 284 (1) (2009) 1–5.
[89] C. Moessinger, K. Klizaite, A. Steinhagen, J. Philippou-Massier, A. Shevchenko, M. Hoch, et al., Two different pathways of phosphatidylcholine synthesis, the Kennedy Pathway and the Lands Cycle, differentially regulate cellular triacylglycerol storage, BMC Cell Biol. 15 (2014) 43.
[90] C. Xu, J. Fan, Links between autophagy and lipid droplet dynamics, J. Exp. Bot. 73 (9) (2022) 2848–2858.
[91] Y.H. Lee, J. Kim, K. Park, M.S. Lee, β-Cell autophagy: mechanism and role in β-cell dysfunction, Mol. Metab. 27S (Suppl) (2019) S92–S103.
[92] J.M. Brown, L.L. Rudel, Stearoyl-coenzyme A desaturase 1 inhibition and the metabolic syndrome: considerations for future drug discovery, Curr. Opin. Lipidol. 21 (3) (2010) 192–197.
[93] M. Huang, X. Yang, Z. Wang, J. Long, A. Wang, Y. Zhang, et al., Lipophagy: a new perspective of natural products in type 2 diabetes mellitus treatment, Diabetes Metab. Syndr. Obes. 14 (2021) 2985–2999.